THE PHOTOMETRIC PROPERTIES OF BRIGHTEST CLUSTER GALAXIES

Thesis by

John Greg Hoessel

In partial fulfillment of the requirements for the Degree of

Doctor of Philosophy

California Institute of Technology

Pasadena, California

1980

(Submitted November 8, 1979)

ACKNOWLEDGMENTS

It is not possible to specifically thank all the individuals who have contributed in some way to this work during its overly long course.

Jim Gunn served as advisor and supplied much guidance throughout my entire career.

J. B. Oke also helped me in many ways, including making available the SIT detector system front end used for most of this work.

Jim Westphal and Jerry Kristian loaned me much of their excellent hardware and software, and also engaged in numerous important and interesting discussions on many subjects.

Without the dedicated efforts of Steve Kent the SIT system, which made this work possible, would never have gotten off the ground.

Bill Sebok contributed many useful software suggestions used in the reduction and analysis of the data.

Don Schneider obtained some of the data used and also made valuable suggestions regarding the analysis.

I wish to thank the Observatory mountain crews for their help in making the observations possible, especially Gary Tuton and Larry Blakee', also Earle Emery.

Elsa-Brita Titchenell contributed much to the final form of this manuscript.

Finally, I would like to acknowledge the financial

support I received from Caltech, the National Science Foundation, and the National Aeronautics and Space Administration.

ABSTRACT

Photometry of a large sample of first-ranked cluster galaxies, obtained with SIT and CCD area photometers, is discussed. The absolute photometric results anchor the bright end of the Hubble diagram; essentially the entire formal error for the method is now due to the distant clusters used. New determinations of the systematic trend of galaxy absolute magnitude with the cluster properties of richness and Bautz-Morgan type are derived.

Structural properties of the galaxies are derived from the surface photometric observations. All the structure data support and are interpreted on the dynamical friction evolution model. Twenty-eight percent of the galaxies have multiple component nuclei; the short lifetimes of such systems provide the best available evidence that ongoing evolution actually occurs. Average magnitude and structure evolution rates are derived and used to estimate corrections to the value of q_o derived from the Hubble diagram. When combined with the expected rate of evolution of the stellar population in the galaxies and accounting for known selection effects in the sample, a true value near the formal value of $q_o = -0.5$ is indicated, suggesting an open universe.

Correlation of the absolute magnitudes with galaxy structure may be used to eliminate the magnitude dependence on cluster richness and Bautz-Morgan type, and remove the bias introduced into cluster samples by selection procedures.

After removal of the trend due to differences in their evolution the dispersion in the magnitudes of those brightest cluster galaxies is reduced to $\sigma = 0\overset{m}{.}21$ and the scatter in their core radii is $\sigma = 22\%$.

CONTENTS

PRELIMINARY REMARKS

This thesis is divided into two chapters, each a self-contained article for submission to the Astrophysical Journal. The research described in Chapter I was done in collaboration with J. E. Gunn and T. X. Thuan.

CHAPTER I

MAGNITUDES FOR 116 GALAXIES

I. INTRODUCTION

The redshift-magnitude relation for the brightest members of rich clusters of galaxies is at present probably the most powerful global test in observational cosmology (Gunn and Oke 1975, hereafter GO; Kristian, Sandage, and Westphal 1978, hereafter KSW). One major remaining source of observational error in the formal value of q_o is inexact knowledge of the mean absolute magnitude of first-ranked galaxies at the present epoch. The purpose of the present study is to reduce this uncertainty, along with investigation of the systematics of the absolute magnitudes with cluster richness class and Bautz-Morgan (BM) type (Bautz and Morgan 1970; Sandage, Kristian, and Westphal 1976, hereafter SKW) for a well-defined set of clusters.

The sample chosen consists of all Abell clusters (Abell 1958) with richness class greater than or equal to one, distance class four or less, and galactic latitude above thirty degrees in absolute value. Additionally, all high latitude richness zero clusters of distance class three or less are included, in order to increase overlap with the low redshift sample of GO and enable study of systematic trends over a wider range of cluster richness. Three clusters have insufficient observational data to warrant inclusion here. A total of 116 first-ranked galaxies are photometered. Red-

shifts for these clusters an analysis of their space distribution are published elsewhere (Thuan and Gunn 1980).

After description of the observations and systematic trends in this new set of photometric data we briefly discuss the implications of these results for the Hubble diagram determination of q_o. Structural properties of a large subset of the galaxies measured here and related evolutionary effects are discussed by Hoessel (1980, Paper II).

II OBSERVATIONAL MATERIAL

Photometric observations were obtained in the green and red (g, r) passbands of the photometric system of Thuan and Gunn (1976). Three instruments were used to collect the data, a pulse-counting photometer, SIT vidicon area photometer, and CCD area photometer. Reduction of the SIT and CCD pictures to the multiaperture magnitudes used here are detailed in Paper II. Enlargements from the Palomar Sky Survey were used to locate the first-ranked galaxy in each cluster. In those cases where no clear choice was evident, several of the brightest galaxies were measured and results for the most luminous included here.

One third of the galaxies in the sample were observed with a two channel pulse-counting photometer at the 1.5-meter Palomar reflector. The instrument and filters were identical to those with which the photometric system was defined. Galaxies were centered visually in one channel, measured in both colors, then centered in the other channel and remeasured. Data from each aperture were reduced separately to outside the atmosphere by transformations derived from observations of at least eight system standard stars each night. The photometric residuals were generally 1-2% and never larger than 3%. Counting statistics for the galaxies were generally 1-2% in each aperture. Final reduced measurements for the two channels were compared; if agreement was inferior to 0.04 mag, the measurements were rejected and the object re-observed. Fifteen galaxies had acceptable measurements

made on more than one night. General agreement between nights was better than 0.04 mag.

Observations were frequently obtained through several size apertures bracketing the desired metric sampling radius of 16 kpc (assuming throughout H_o = 60 km s^{-1} Mpc^{-1} and q_o = 1/2). For objects with such multiaperture data, including all SIT and CCD observations, the measurements were interpolated to this standard radius. Other observations were aperture corrected following the procedure of GO. Results of Paper II indicate a mean value of α = 0.49 for the present sample which was used.

Redshifts, observation angular size and physical radius, magnitudes, colors, and aperture corrections are listed in columns 7-13 of Table 1. No entry in column 10 signifies that the data were interpolated to the correct radius of 16 kpc. Coordinates for the galaxies observed, accurate to $\pm$20 arcseconds may be found in the second column. Cluster galactic latitude, Abell richness class, and Abell distance class are columns 3-5. Cluster BM types in column 6 are lifted from Leir and van den Bergh (1977).

The magnitudes in column 15 are on the VI system defined by GO; VI is the monochromatic magnitude at 5456 Å in the galaxy's rest frame, corrected for galactic obscuration via the reddening-free polar cap model of Sandage (1972). This magnitude was derived from the intermediate-band g and r magnitudes in the following fashion: the difference VI-g and VI-r are calculated as a function of redshift for a

standard galaxy (NGC 4889 in this case) from multichannel spectrophotometer data of high quality, using the effective wavelengths for the passbands which are shown in Thuan and Gunn (1976). These corrections are applied to a sample galaxy to calculate two values, VI(g) and VI(r). If the intrinsic colors of the sample galaxy agree exactly with those of NGC 4889, these two magnitudes will agree exactly as well. In general they are different by a few hundredths of a magnitude. The final value is obtained by a weighted mean of the two values, the weight being inversely proportional to the difference between the effective wavelength of the filters and 5456(1+z). This procedure is similar to the usually used K-correction, but is an interpolation, since 5456(1+z) is, for this sample, between the effective wavelengths for g and r. The values of VI are limited in accuracy almost entirely by the errors in the photometry. Absolute intrinsic magnitudes, listed in column 16 of Table 1 were calculated assuming H_0 = 60 km s^{-1} Mpc^{-1} and $q_o = 1/2$. The final column lists the type and number of observations available for each object, with T indicating photometer, S for SIT, and C meaning CCD.

Seven galaxies were measured both with the phototubes and the SIT system. Comparison of these results yields a mean deviation for the seven of 0.00 mag with an rms scatter of 0.03 mag. These objects were on average slightly brighter than the sample average. Repeat observations of the faintest galaxies in the sample on different nights with the SIT

system generally agree to 0.04 mag. Three faint galaxies from the sample along with first-ranked galaxies in two more distant clusters ($z \sim 0.25$) were observed both with the SIT and CCD. These five comparisons show a mean deviation of 0.02 mag with a scatter of 0.04 mag. We conclude from these results that the photometric data set presented in Table 1 is free of detectable systematic measurement trends and is self-consistent to 0.04 mag.

III DISCUSSION

The remarkably small dispersion in absolute aperture magnitude of first-ranked cluster galaxies is a subject of much interest. Special formation (Sandage 1976) or evolutionary (e.g., Hausman and Ostriker 1978) processes have been proposed to account for this similarity. The absolute intrinsic magnitudes from Table 1 are histogrammed in Figure 1. The mean absolute magnitude for this nearly normal distribution is $\langle M_{VI} \rangle = -22.68 \pm 0.03$ mag, with a dispersion of 0.35 mag. A similar value for the scatter is found by KSW.

Available data allow the study of the systematics of absolute magnitude with the cluster properties of Abell richness and BM type. Absolute magnitudes subdivided by richness class are plotted in Figure 2. A trend towards brighter brightest galaxies with increasing cluster richness is evident. Mean absolute magnitudes for each class listed in Table 2 are most consistent with a brightening of 0.10 mag per class. SKW find a 0.05 mag per class gradient from less complete data with a wider range of richness and redshift. We do not believe these two values to be inconsistent, given the errors in each.

Sandage and Hardy (1973) have shown that absolute aperture magnitudes for brightest galaxies correlate with cluster BM type. Data for our sample, subdivided by BM class are histogrammed in Figure 3. Mean absolute magnitudes for each class are the content of Table 3. The difference from class I to III amounts to 0.41 mag where KSW find a value of

0.54 mag. Changes with class agree well except for the bright end where KSW find a larger effect. The slow surface brightness declines with radius for cD galaxies and the larger metric diameters of KSW combine to explain this. After applying corrections to the absolute magnitudes for both richness and BM type, derived from Tables 2 and 3, we obtain a dispersion of $\sigma = 0.30$ mag in agreement with the result of KSW. More extensive discussion of the nature of these effects is deferred to Paper II.

The mean absolute magnitude for the present sample is 0.07 mag brighter than for the low redshift galaxies of GO. Twenty-nine galaxies are in common between the two lists. New measurements average 0.05 mag brighter than the old, which were obtained from broadband V photometry using rather heterogeneous data. The remainder of the discrepancy is consistent with the fact that the new sample is somewhat richer than the old. A redshift - apparent magnitude diagram for the present data, along with the distant sample of GO (excluding 3C 295) is shown as Figure 4. Detailed discussion of the Hubble diagram will be deferred until a forthcoming reanalysis including a much larger, fainter, and more homogeneous set of faint clusters is completed. Briefly stated, the implications of the new low redshift data are, as applied to the GO case of 3C 295 out, no evolution, a change of -0.40 in the formal value to $q_o = -0.55$, along with reduction of the formal error from $\sigma_{q_o} = 0.57$ to $\sigma_{q_o} = 0.45$. Thus even a modest change in the bright end data can yield a large change

in the global determination of q_o. The reduction of the uncertainty in the mean absolute magnitude at the present epoch by the observations reported here makes such large changes unlikely in the future. The formal errors for q_o are now essentially dependent only on the faint sample. New CCD technology is resulting in dramatic reduction of the effort necessary to improve data for the faint sample. We expect shortly to have sufficient data to reduce the formal error to below $\sigma_{q_o} = 0.25$. Uncertainty in the true value of the deceleration is of course much larger than even the present formal error, due primarily to the poorly understood luminosity evolution of the brightest galaxies and systematic bias in the cluster samples. These problems are addressed in Paper II.

TABLE 1

Observed Properties of Low Redshift Sample

Abell	α (1950.0)	δ	b^{II}	R	D	BM	z	log z	$^{2}\gamma_{obs}$	radius	g	g-r	Ap corr	Red corr	V I	M_{VI}	Obs
(1)	(2)		(3)	(4)	(5)	(6)	(7)	(8)	(9)	(10)	(11)	(12)	(13)	(14)	(15)	(16)	(17)
21...	00 18 03	+28 23 12	-33.7	1	4	I	0.0948	-1.024	16.32		15.90	0.63		0.145	15.13	-23.30	S
76...	00 36 50	+06 27 00	-56.2	0	3	II-III	0.0377	-1.423	37.36		14.21	0.58			13.80	-22.61	T6
85...	00 39 18	-09 34 21	-72.1	1	4	I	0.0556	-1.255	26.10		14.74	0.54			14.29	-22.98	S2
88...	00 40 22	-26 21 28	-87.8	1	3	III	0.1086	-0.964	14.56		16.72	0.77			15.95	-22.79	S2
104...	00 47 11	+24 10 52	-38.4	1	4	II-III	0.0822	-1.085	18.44		16.03	0.62		0.10	15.35	-22.76	S2
119...	00 53 42	-01 31 22	-64.1	1	3	II-III	0.0446	-1.351	31.95		14.50	0.57			14.07	-22.71	S,T10
121...	00 55 06	-07 17 05	-69.8	1	4	III	0.1048	-0.979									
147...	01 05 34	+01 55 00	-60.5	0	3	III	0.0441	-1.356	32.28		14.90	0.48			14.51	-22.23	T4
151...	01 06 22	-15 42 24	-77.6	1	3	II	0.0526	-1.279	27.45		14.37	0.43			13.99	-23.15	S
154...	01 08 17	+17 23 23	-45.0	1	3	II	0.0612	-1.213	23.93		14.97	0.58		0.04	14.44	-23.01	S
166...	01 12 06	-16 32 55	-77.9	1	4	III	0.1156	-0.937	13.83		17.28	0.63			16.60	-22.26	S2,C
168...	01 12 43	-00 03 17	-62.1	2	3	II-III	0.0457	-1.340	31.24		14.72	0.56			14.29	-22.54	S2
189...	01 20 54	+01 25 32	-60.2	1	4	III	0.0349	-1.457	40.16		14.57	0.55			14.18	-22.05	S
193...	01 22 31	+08 26 09	-53.3	1	4	II	0.0478	-1.321	29.97		14.53	0.58			14.09	-22.84	S
194...	01 23 24	-01 36 00	-63.1	0	1	II	0.0178	-1.749	76.48		12.27	0.49			11.95	-22.83	T8
225...	01 36 06	+18 34 06	-42.6	1	4	II-III	0.0692	-1.159	21.45		15.64	0.60		0.07	15.04	-22.69	S,T4
246...	01 42 06	+05 33 19	-54.6	1	4	II-III	0.0753	-1.123	19.91		16.31	0.65			15.73	-22.18	S1,C
274...	01 52 28	-06 30 16	-64.3	3	4	III	0.1289	-0.889	12.66		16.84	0.61			16.15	-22.97	C
277...	01 53 22	-07 39 13	-65.0	1	3	III	0.0947	-1.024	16.33		16.16	0.58			15.58	-22.85	S,C
389...	02 49 12	-25 09 18	-63.0	2	4	II	0.1160	-0.935	13.79		16.64	0.67			15.93	-22.95	S
399...	02 55 09	+12 50 02	-39.5	1	3	I-II	0.0725	-1.139	20.58		15.87	0.73		0.09	15.16	-22.66	S2
400...	02 55 05	+05 49 15	-44.9	1	1	II-III	0.0231	-1.636	59.47		13.66	0.74		0.05	13.16	-22.16	T4
401...	02 56 12	+13 23 03	-38.9	2	3	I	0.0752	-1.124	19.93		15.79	0.69		0.10	15.09	-22.82	S
415...	03 04 33	-12 18 45	-54.9	1	4	II											
496...	04 31 18	-13 22 37	-36.5	1	3	I	0.0326	-1.487	42.83		13.90	0.57		0.13	13.39	-22.71	S
500...	04 36 45	-22 13 07	-38.5	1	4	III	0.0666	-1.176	22.19		15.49	0.52		0.10	14.92	-22.74	S2
514...	04 46 16	-20 30 12	-36.0	1	3	II-III	0.0697	-1.157	21.31		15.79	0.58		0.12	15.21	-22.55	S
634...	08 11 38	+58 28 29	33.8	0	3		0.0266	-1.575	57.46	15.14	13.79	0.56	0.07	0.16	13.32	-22.35	T6
671...	08 25 27	+30 36 02	33.6	0	3	II-III	0.0497	-1.304	28.96	16.03	14.50	0.55	0.01	0.15	13.92	-23.10	T2
779...	09 16 46	+33 57 29	44.9	0	1	I-II	0.0201	-1.697	67.99		12.49	0.53		0.05	12.09	-22.92	T4
787...	09 22 21	+74 39 50	36.2	2	4	II	0.1355	-0.868	12.17		17.09	0.83		0.11	16.09	-23.13	S3
957...	10 11 05	-00 41 09	42.9	1	4	I-II	0.0437	-1.359	32.56		14.33	0.57		0.07	13.83	-22.91	T8
978...	10 17 56	-06 16 56	40.4	1	3	II	0.0527	-1.278	28.96	16.91	14.87	0.56	0.04	0.08	14.36	-22.78	T2
993...	10 19 26	-04 38 23	42.2	0	3	III	0.0530	-1.276	28.96	17.00	14.73	0.53	0.04	0.07	14.26	-22.88	T2
1020...	10 25 11	+10 42 04	52.3	1	4	II-III	0.0650	-1.187	22.68		15.91	0.56			15.43	-22.16	S
1035...	10 29 18	+40 32 12	58.5	2	3	II-III	0.0799	-1.098	20.94	17.73	15.69	0.62	0.06		15.17	-22.88	T2
1126...	10 51 10	+17 06 35	61.0	1	4	I-II	0.0828	-1.082	18.33		15.62	0.74			14.97	-23.16	T4
1139...	10 55 37	+01 51 49	53.2	0	3	III	0.0376	-1.425	41.08	17.55	14.61	0.53	0.06		14.27	-22.14	T2
1185...	11 07 56	+29 02 41	67.8	1	2	II	0.0349	-1.457	40.16		13.81	0.53			13.43	-22.80	S,T4
1187...	11 08 25	+39 52 23	65.9	1	3	III	0.0791	-1.102	19.07		15.67	0.56			15.14	-22.88	S
1213...	11 13 32	+29 40 16	69.0	1	2	III	0.0484	-1.315	29.63		14.69	0.58			14.24	-22.69	T4
1216...	11 15 36	-04 08 46	51.1	1	4	III	0.0524	-1.281	27.55		15.38	0.56			14.92	-22.18	S
1228...	11 18 41	+34 38 23	69.4	1	1	II-III	0.0344	-1.463	40.71		14.41	0.51			14.03	-22.14	T4
1238...	11 20 22	+01 23 23	56.4	1	4	III	0.0716	-1.145	20.81		15.84	0.57			15.33	-22.49	S
1254...	11 22 00	+71 10 50	44.5	1	3	III	0.0628	-1.202	23.39		15.61	0.65		0.05	15.03	-22.49	S

TABLE 1 (continued)

Abell	α (1950.0) δ	b^{II}	R	D	BM	z	log z	$2\gamma_{obs}$	radius	g	g-r	Ap corr	Red corr	V I	M_{VI}	Obs
(1)	(2)	(3)	(4)	(5)	(6)	(7)	(8)	(9)	(10)	(11)	(12)	(13)	(14)	(15)	(16)	(17)
1257...	11 23 34 +35 36 29	70.5	0	3		0.0339	-1.470									
1291...	11 29 38 +56 14 25	57.8	1	3	III	0.0586	-1.232	24.89		15.87	0.55			15.41	-21.97	S
1318...	11 32 52 +55 13 22	59.0	1	3	II	0.0189	-1.724	57.46	12.74	13.39	0.49	-0.12		12.94	-21.96	T6
1364...	11 40 57 -01 27 54	56.8	1	4	III	0.1070	-0.971	14.74		16.70	0.70			15.99	-22.71	S
1365...	11 41 52 +31 09 41	74.9	1	4	III	0.0763	-1.118	19.68		15.92	0.61			15.36	-22.58	S
1367...	11 41 28 +20 14 03	73.0	2	1	II-III	0.0205	-1.688	57.46	13.78	13.01	0.46	-0.09		12.63	-22.38	T2
1377...	11 44 42 +56 00 22	59.1	1	3	III	0.0509	-1.293	28.29		14.99	0.58			14.54	-22.52	S2
1382...	11 45 21 +71 41 00	44.8	1	4	II	0.1046	-0.981	15.02		16.54	0.69		0.05	15.80	-22.86	S
1383...	11 45 26 +54 55 36	60.2	1	4	III	0.0598	-1.223	20.94	13.71	15.81	0.55	-0.08		15.26	-22.16	T2
1399...	11 48 51 -02 51 31	56.5	2	4	III	0.0913	-1.039	16.85		16.54	0.57			15.97	-22.37	S
1412...	11 53 22 +73 41 38	43.1	2	4	III	0.0839	-1.076	18.12		16.40	0.60		0.05	15.77	-22.39	S
1436...	11 57 40 +56 32 02	59.5	1	3	III	0.0646	-1.190	22.80		15.34	0.56			14.86	-22.73	S
1468...	12 02 54 +51 37 26	64.2	1	4	I	0.0853	-1.069	17.86		16.27	0.60			15.69	-22.50	S
1474...	12 05 34 +15 20 22	74.2	1	4	III	0.0778	-1.109	19.35		16.43	0.58			15.89	-22.11	S
1496...	12 11 19 +59 36 12	57.2	1	4	III	0.0961	-1.017	16.13		16.64	0.51			16.09	-22.37	S
1541...	12 25 00 +09 04 46	70.9	1	4	I-II	0.0892	-1.050	17.19		16.12	0.68			15.48	-22.81	S
1644...	12 54 32 -17 09 12	45.5	1	4	II	0.0456	-1.341	31.30		14.76	0.58		0.04	14.28	-22.55	S
1651...	12 56 48 -03 56 16	58.6	1	4	I-II	0.0842	-1.075	18.06		15.88	0.62			15.29	-22.87	S
1656...	12 57 45 +28 15 16	88.0	2	1	II	0.0230	-1.638	57.46	15.40	12.59	0.53	-0.02		12.21	-23.11	T4
1691...	13 08 51 +39 29 23	77.2	1	3	II	0.0722	-1.142	20.66		15.37	0.52			14.88	-22.94	S
1749...	13 27 06 +37 52 49	76.8	1	4	II	0.0562	-1.250	25.85		14.89	0.58			14.41	-22.86	T6
1767...	13 34 21 +59 27 08	57.0	1	4	II	0.0712	-1.148	20.91		15.48	0.62			14.93	-22.86	T4
1773...	13 39 35 +02 29 22	62.3	1	3	III	0.0776	-1.110	19.39		15.62	0.57			15.09	-22.91	S
1775...	13 39 30 +26 37 56	78.7	2	4	I	0.0718	-1.144	20.76		15.47	0.60			14.94	-22.88	S
1793...	13 46 02 +32 30 00	76.6	1	4	III	0.0849	-1.071	17.93		16.23	0.55			15.68	-22.51	S
1795...	13 46 35 +26 50 16	77.2	2	4	I	0.0631	-1.200	23.29		15.19	0.51			14.73	-22.79	S
1809...	13 50 36 +05 23 35	63.6	1	4	II	0.0788	-1.104	20.94	17.51	15.45	0.67	0.05		14.90	-23.12	T2
1831...	13 56 59 +28 13 22	75.0	1	3	III	0.0749	-1.126	20.00		15.40	0.59			14.87	-23.04	S
1837...	13 58 57 -10 54 14	48.1	1	4	I-II	0.0376	-1.425	28.96	12.37	14.97	0.62	-0.13	0.02	14.38	-22.03	T4
1904...	14 20 21 +48 47 29	62.3	2	3	II-III	0.0719	-1.143	20.73		15.20	0.54			14.70	-23.12	S
1913...	14 23 58 +17 01 44	65.6	1	4	III	0.0533	-1.273	27.12		15.27	0.57			14.81	-22.33	T4
1927...	14 28 51 +25 51 27	67.7	1	4	I-II	0.0740	-1.131	20.21		16.12	0.69			15.52	-22.36	S
1983...	14 50 35 +16 54 19	60.1	1	3	III	0.0458	-1.339	31.17		15.22	0.46			14.84	-21.99	S
1991...	14 52 14 +18 50 42	60.5	1	3	I	0.0589	-1.230	24.77		15.19	0.54			14.74	-22.64	S
1999...	14 53 21 +54 34 39	54.8	1	4	II-III	0.1032	-0.986	15.19		16.41	0.62			15.77	-22.84	S
2005...	14 56 30 +28 03 44	61.8	2	4	III	0.1251	-0.903	12.97		16.86	0.66			16.14	-22.91	S
2022...	15 02 09 +28 41 20	60.7	1	3	III	0.0565	-1.248	25.72		15.13	0.59			14.65	-22.62	S
2028...	15 07 01 +07 44 17	51.9	1	4	II-III	0.0772	-1.112	19.37		15.64	0.65			15.05	-22.92	S
2029...	15 08 27 +05 56 35	50.6	2	4	I	0.0777	-1.110	19.37		15.12	0.61			14.57	-23.43	S
2040...	15 10 20 +07 37 42	51.2	1	4	III	0.0456	-1.341	31.30		15.21	0.61			14.76	-22.07	S
2048...	15 12 44 +04 34 02	48.9	1	4	III	0.0945	-1.025	16.36		16.15	0.69		0.02	15.47	-22.94	S
2052...	15 14 12 +07 12 26	49.7	0	3	I-II	0.0351	-1.455	41.08	16.45	14.13	0.57	0.02	0.01	13.73	-22.50	T4
2061...	15 19 17 +30 51 23	57.2	1	4	III	0.0782	-1.107	19.26		15.46	0.59			14.91	-23.09	S
2063...	15 20 39 +08 47 14	49.7	1	3	II	0.0337	-1.472	41.51		14.10	0.51		0.01	13.72	-22.45	S
2065...	15 20 18 +27 53 49	56.6	2	3	III	0.0722	-1.142	20.66		15.73	0.54			15.23	-22.59	S

TABLE 1 (continued)

Abell	α (1950.0)	δ	b^{II}	R	D	BM	z	log z	$^{2Y}_{obs}$	radius	g	g-r	Ap corr	Red corr	V I	M_{VI}	Obs
(1)	(2)		(3)	(4)	(5)	(6)	(7)	(8)	(9)	(10)	(11)	(12)	(13)	(14)	(15)	(16)	(17)
2067...	15 21 06	+31 03 27	56.8	1	4	III	0.0726	-1.139	20.56		16.10	0.52			15.62	-22.23	S
2079...	15 25 40	+29 06 39	55.5	1	3	II-III	0.0657	-1.182	22.46		15.15	0.56			14.66	-22.97	S
2089...	15 30 43	+28 12 09	54.4	1	4	II	0.0743	-1.129	20.94	16.63	15.59	0.67	0.02		15.02	-22.86	T4
2092...	15 31 14	+31 18 35	54.6	1	4	II-III	0.0669	-1.175	22.10		15.82	0.53			15.35	-22.31	S
2107...	15 37 26	+21 56 56	51.5	1	4	I	0.0421	-1.376	33.70		14.23	0.58			13.79	-22.84	S,T4
2124...	15 43 05	+36 16 31	52.3	1	3	I	0.0671	-1.173	22.04		15.30	0.57			14.79	-22.87	S
2142...	15 56 10	+27 23 36	48.7	2	4	II	0.0911	-1.041	16.88		16.49	0.61		0.02	15.88	-22.46	S
2147...	15 59 58	+16 06 20	44.5	1	1	III	0.0377	-1.424	37.36		14.26	0.53		0.05	13.82	-22.59	S,T4
2151...	16 02 23	+17 51 54	44.5	2	1	III	0.0360	-1.444	39.01		14.20	0.55		0.05	13.75	-22.55	S2,T6
2152...	16 03 13	+16 34 35	44.0	1	1	III	0.0444	-1.353	32.35		14.75	0.54		0.05	14.29	-22.45	T6
2162...	16 10 31	+29 35 08	45.4	0	1		0.0318	-1.498	41.08	14.99	13.95	0.54	-0.03	0.04	13.49	-22.55	T6
2175...	16 18 34	+30 01 08	44.4	1	4	II	0.0978	-1.010	15.90		16.54	0.78		0.05	15.76	-22.74	S
2197...	16 26 32	+41 01 42	43.8	1	1	III	0.0303	-1.519	45.90		13.24	0.48		0.06	12.82	-23.08	S3
2199...	16 26 57	+39 40 31	43.7	2	1	I	0.0312	-1.506	44.64		13.14	0.45		0.06	12.74	-23.25	S
2255...	17 12 10	+64 07 00	35.0	2	3	II-III	0.0747	-1.127	20.05		15.62	0.54		0.13	14.99	-22.92	S
2256...	17 06 31	+78 47 29	31.7	2	3	II-III	0.0550	-1.260	26.36		14.56	0.55		0.18	13.93	-23.30	S
2328...	20 45 21	-17 59 50	-33.6	2	4		0.1470	-0.852	11.82		16.91	0.73		0.14	15.95	-23.37	S2
2347...	21 26 41	-22 25 12	-44.2	1	4	III	0.1196	-0.922	13.45		17.00	0.70		0.05	16.22	-22.73	S
2382...	21 49 12	-15 56 22	-46.9	1	4	II-III	0.0648	-1.188	22.74		15.84	0.74		0.03	15.22	-22.37	S
2384...	21 49 35	-19 46 47	-48.4	1	4	II-III	0.0943	-1.026	16.39		16.51	0.59		0.02	15.90	-22.51	S
2399...	21 54 54	-08 02 02	-44.6	1	3	III	0.0587	-1.231	24.85		15.52	0.57		0.05	15.00	-22.38	S
2410...	21 59 04	-10 07 58	-46.6	1	4	III	0.0806	-1.094	18.76		15.79	0.60		0.03	15.20	-22.88	S
2457...	22 33 08	+01 13 34	-46.6	1	4	I-II	0.0597	-1.224	24.47		15.11	0.63		0.03	14.56	-22.86	S
2634...	23 36 00	+26 45 01	-33.1	1	1	II	0.0315	-1.502	44.24		13.62	0.57		0.16	13.06	-22.91	T6
2657...	23 42 25	+08 55 02	-50.3	1	3	III	0.0414	-1.383	34.23		15.38	0.68			14.90	-21.68	S2
2666...	23 48 21	+26 52 00	-34.1	0	1	I	0.0273	-1.564	50.69		13.03	0.41		0.15	12.56	-23.11	T12
2670...	23 51 40	-10 41 43	-68.5	3	4	I-II	0.0774	-1.111	19.43		15.53	0.61			14.97	-23.00	S2,T6
2675...	23 53 10	+11 03 59	-49.1	1	4	II	0.0726	-1.139	20.56		15.78	0.59		0.01	15.24	-22.61	S
2700...	00 01 17	01 46 25	-58.6	1	4	II	0.0978	-1.010	15.90		16.27	0.63			15.64	-22.86	S

TABLE 2

Mean Absolute Magnitudes for Each Richness Class

Richness	$< M_{VI} >$	σ
0...	-22.66 ± 0.10	0.34
1...	-22.62 ± 0.04	0.34
2...	-22.86 ± 0.07	0.34
3...	-22.99	

TABLE 3

Mean Absolute Magnitudes for Each Bautz-Morgan Class

BM	$< M_{VI} >$	σ
I.....	-22.93 ± 0.08	0.27
I-II.....	-22.74 ± 0.10	0.33
II.....	-22.81 ± 0.06	0.28
II-III...	-22.64 ± 0.07	0.34
III.....	-22.52 ± 0.06	0.34

REFERENCES

Abell, G. O. 1958, Ap. J. Suppl., 3, 211.

Bautz, L. P. and Morgan, W. W. 1970, Ap. J. (Letters), 162, L149.

Gunn, J. E. and Oke, J. B. 1975, Ap. J. 195, 255.

Hausman, M. A. and Ostriker, J. P. 1978, Ap. J., 224, 320.

Hoessel, J. G. 1980, in preparation (Paper II).

Kristian, J., Sandage, A., and Westphal, J. A. 1978, Ap. J., 221, 383.

Leir, A. A. and van den Bergh, S. 1977, Ap. J. Suppl., 34, 381.

Sandage, A. 1972, Ap. J., 178, 1.

———— 1976, Ap. J., 205, 6.

Sandage, A. and Hardy, E. 1973, Ap. J., 183, 743.

Sandage, A., Kristian, J., and Westphal, J. A. 1976, Ap. J., 205, 688.

Thuan, T. X. and Gunn, J. E. 1976, PASP, 88, 543.

———————————— 1980, in preparation.

FIGURE 1

Histogram of absolute intrinsic magnitudes for 116 first-ranked cluster galaxies. The Gaussian has the same mean ($\langle M_{VI} \rangle$ = -22.68 mag) and dispersion (σ = 0.35 mag) as the data.

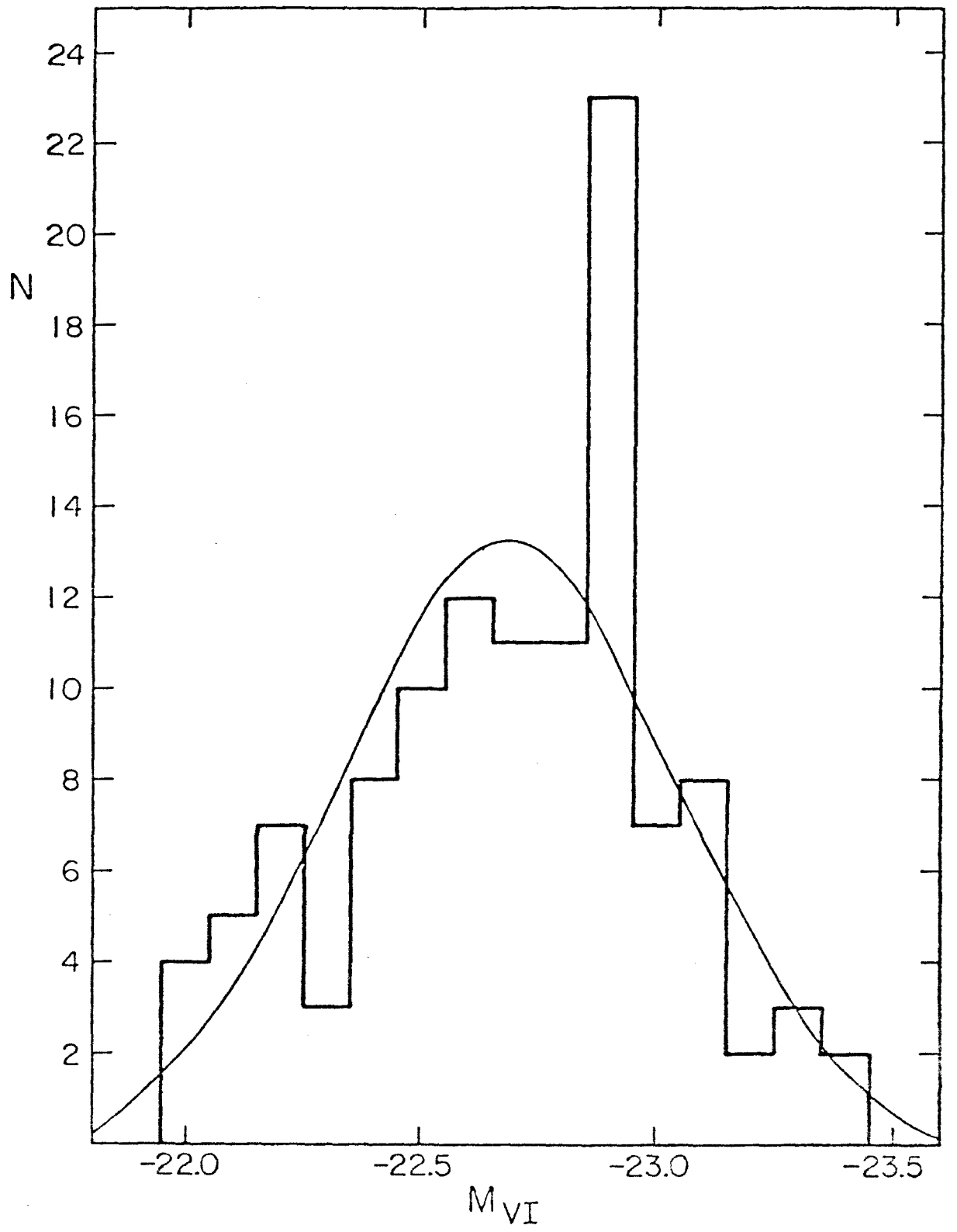
N
24
22
20
18
16
14
12
10
8
6
4
2
-22.0
-22.5
-23.0
-23.5
M VI

FIGURE 2

Absolute intrinsic magnitudes for brightest galaxies binned by cluster richness class. Mean absolute magnitudes for each class are listed in Table 2.

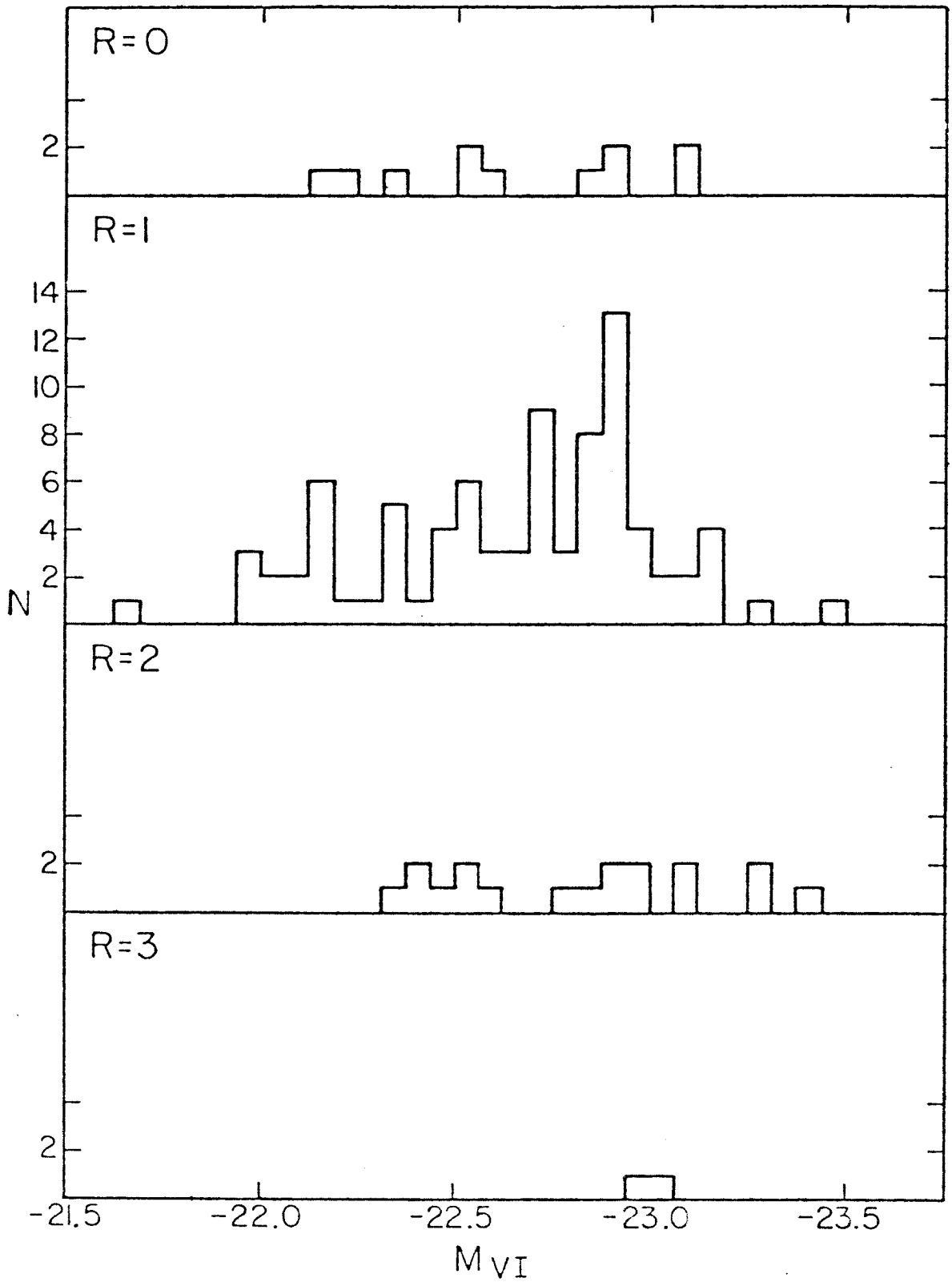
R=0
2
R=1
14
12
10
8
6
4
2
N
R=2
2
R=3
2
-21.5
-22.0
-22.5
-23.0
-23.5
M VI

FIGURE 3

Absolute-intrinsic magnitudes for brightest galaxies binned by cluster Bautz-Morgan type. Mean absolute magnitudes for each class are listed in Table 3.

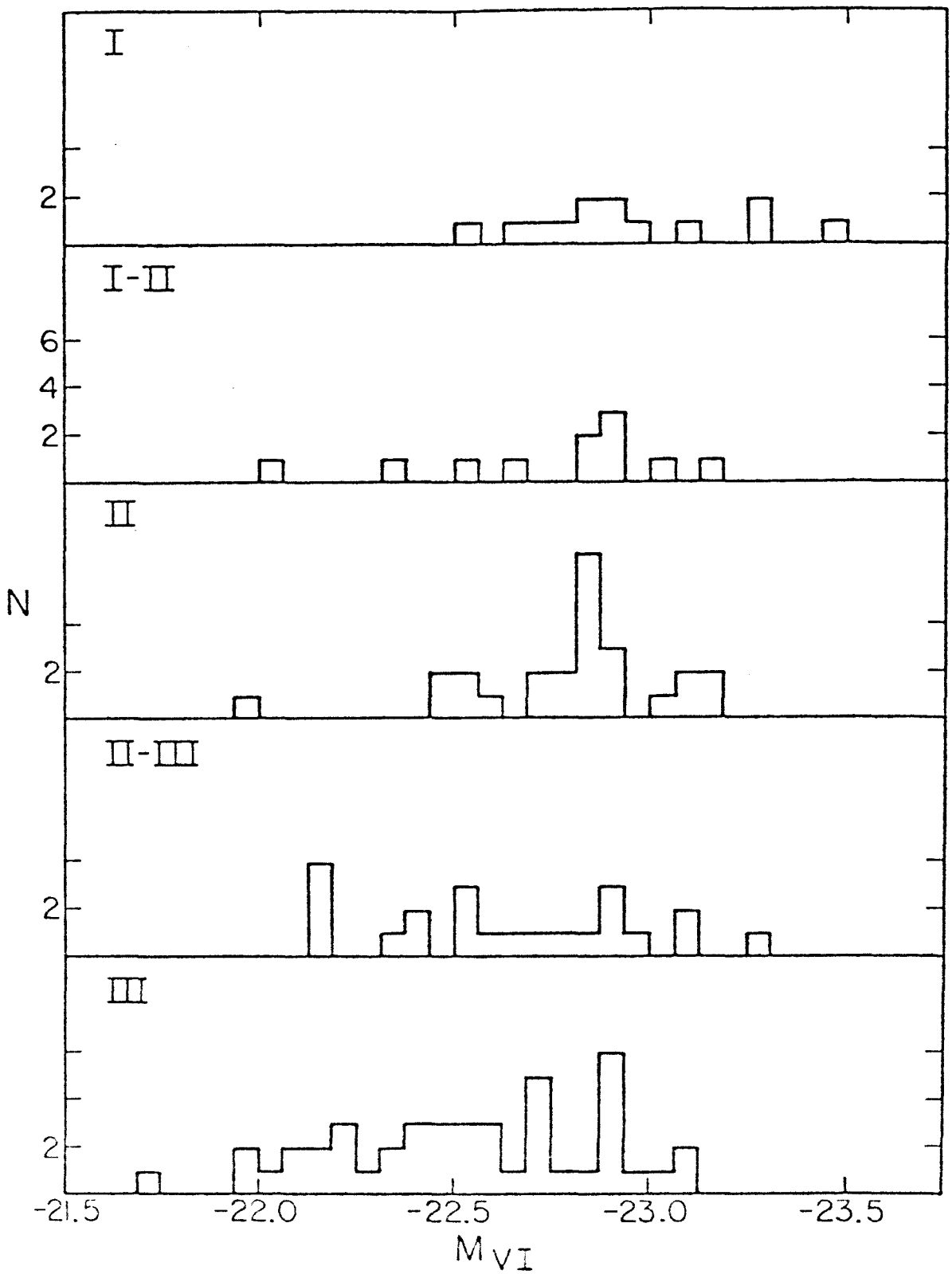
I
2
I-II
6
4
2
II
N
2
II-III
2
III
2
-21.5
-22.0
-22.5
-23.0
-23.5
M VI

FIGURE 4

Hubble diagram for the present data along with the faint sample of GO. A formal value of $q_o = -0.55$ is indicated, with an error of $\sigma_{q_o} = 0.45$.

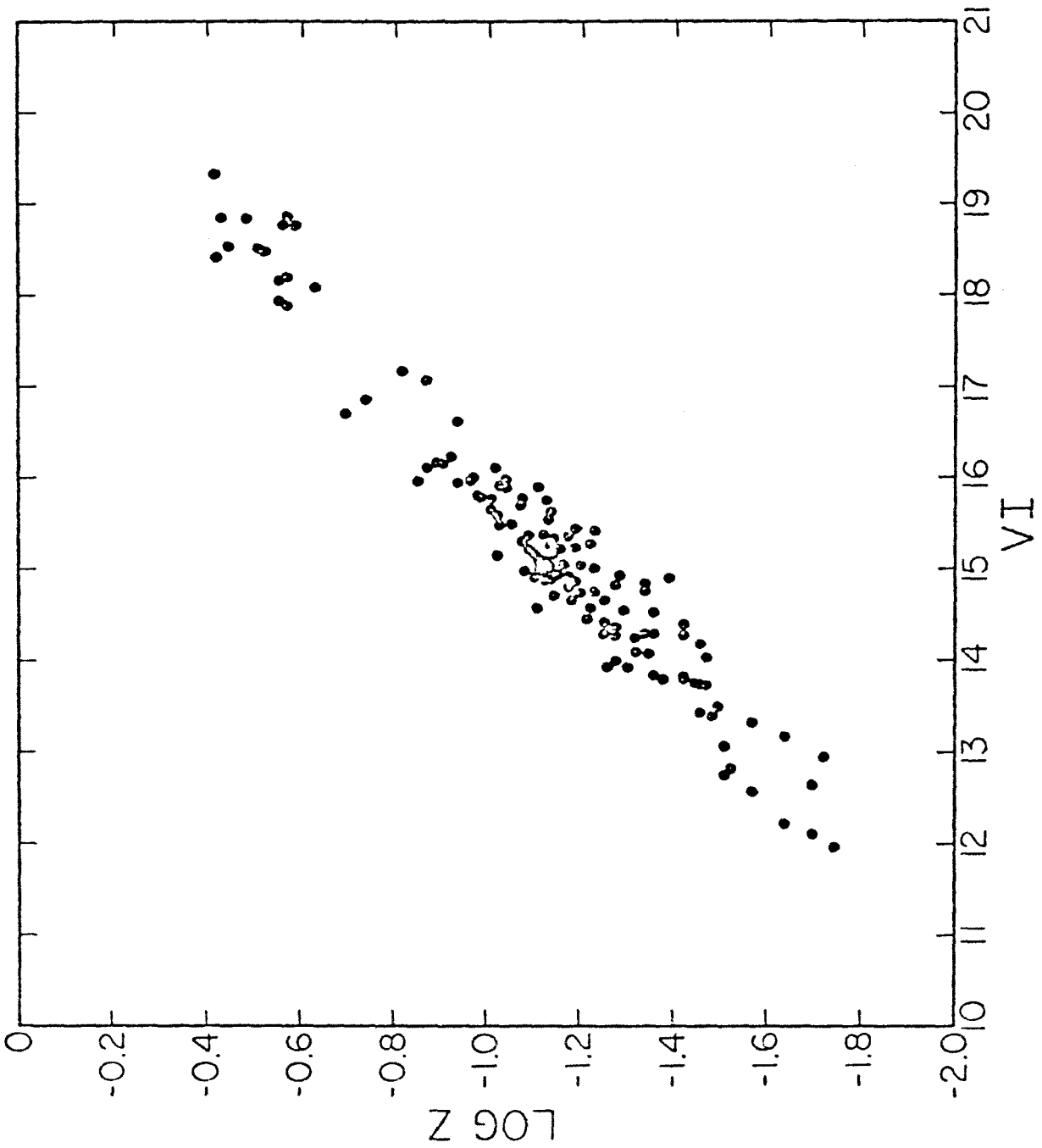
LOG Z
0
-0.2
-0.4
-0.6
-0.8
-1.0
-1.2
-1.4
-1.6
-1.8
-2.0
VI
10
11
12
13
14
15
16
17
18
19
20
21

CHAPTER II

SIT AND CCD SURFACE PHOTOMETRY AND DYNAMICAL EVOLUTION

I. INTRODUCTION

The remarkably small scatter in the absolute magnitudes of first ranked cluster galaxies (e.g., Sandage 1972, Hoessel, Gunn, and Thuan 1980, hereafter cited as Paper I), which makes the Hubble diagram a powerful probe for observational cosmology, has been attributed to some special formation or evolutionary process (Sandage 1976, Dressler 1978a). One such process, the dynamical merger of cluster members to form the giant, has been the subject of considerable theoretical study (Ostriker and Tremaine 1975, White 1976, Gunn and Tinsley 1976, hereafter GT, Ostriker and Hausman 1977, hereafter OH, and Hausman and Ostriker 1978, hereafter HO). Observational support for this model is available from the study of first ranked galaxy structure (Oemler 1976), dynamics (Dressler 1979), and cluster luminosity functions (Dressler 1978b). A thorough understanding of its nature, and the rate at which this process occurs is essential, since it generates a systematic evolution of the absolute luminosities of brightest cluster galaxies (GT), an effect which must be removed before meaningful results for the deceleration can be obtained.

The present work was undertaken in order better to understand the details of this evolutionary process and to calibrate its importance for observational cosmological methods. The theoretical results suggest that the dynamical friction-induced cannibalism not only alters the luminosity of the brightest galaxy; it also produces

strong changes in the galaxy's structure (changing it from a normal elliptical galaxy to a cD system). Both luminosity and structure information are provided by the observational technique of surface photometry. To date such data (detailed in Section II) are available for the central regions of the brightest galaxies in 108 nearby Abell clusters, chosen randomly from the sample defined in Paper I. The structure data are parameterized by simple model galaxies; the results are listed and interpreted in Section III. Implications of these results for cosmology are discussed in Section IV. Future papers in this series will deal with the characteristics of the faint outer envelopes of brightest cluster galaxies, and correlations of galaxy structure with cluster structure.

II. OBSERVATIONS AND REDUCTIONS

The majority of the surface brightness observations reported here were obtained with a SIT vidicon area photometer at the 1.5-meter Palomar telescope. Characteristics of this instrument are detailed by Kent (1979). The system produces a digital picture of 256x256 square pixels with 0.55 arcsecond separation. Several frames were obtained of each of the 108 galaxies. Generally five minute green and red exposures (on the system of Thuan and Gunn 1976) taken under photometric sky conditions were supplemented by two additional red frames with integration times adjusted according to the galaxy's luminosity. In every case the

noise due to sky photon statistics exceeded the instrumental noise.

Five relatively faint galaxies were observed with a CCD system (described by Young et al. 1978) at the prime focus of the 5-meter Hale telescope. Ten minute exposures in both the green and red were obtained of the first-ranked galaxies in the clusters A 166, A 246, A 274, A 227 and A 2328.

The raw picture data were reduced to multiaperture magnitudes by the following procedure: Zero exposure erase frames taken throughout each night were subtracted from all other frames pixel by pixel. Dark emission during the short integrations used here is negligible in both instruments. Several flat field exposures of a uniformly illuminated patch on the inside of the dome were made through the telescope in each color each night. Sky exposures were divided pixel by pixel by the averaged normalized flat field of appropriate color. Prints of six red frames so treated are shown as figure 1. Sky background on each frame was determined by histogramming all pixels by data number and locating the peak value by a simple parabolic fit. This value was then subtracted from each pixel. The center of each object to be photometered was estimated by eye; then improved by an automated two-dimensional centering algorithm. Instrumental magnitudes were synthesized in circular apertures about this location.

Frames of system standard stars, obtained each night, were treated identically to the galaxy pictures. RMS resid-

uals to the transformations to the standard star values were less than 0.04 mag for the SIT and 0.01 mag for the CCD. Galaxy magnitudes were reduced to outside the atmosphere utilizing these derived transformations. Further description of the absolute photometric results is the subject of Paper I.

Surface brightness profiles, derived by differencing the multiaperture intensities, are shown in figure 2 for six galaxies covering the range of observed size and shape in the sample. Throughout this paper all surface brightnesses are in units of red magnitudes per square arcsecond. Previous work on brightness profiles of luminous elliptical galaxies (e.g. Oemler 1976, Kormendy 1977) suggests that the interior regions may be adequately described by Hubble intensity laws. We choose to parameterize our observations by a modified Hubble law of the form

$$I(\gamma) = \frac{I_c}{1+\gamma^2/\beta^2} \qquad (1)$$

where I_c is the central intensity, β the core radius and γ the angular distance from the center. The luminosity contained within a projected radius γ is

$$L_\gamma = \pi I_c \beta^2 \ell n (1+\gamma^2/\beta^2) \qquad (2)$$

yielding a magnitude of

$$m_\gamma = \mu_c - 2.5 \log [\pi \beta^2 \ell n(1+\gamma^2/\beta^2)] \quad (3)$$

with μ_c denoting the central surface brightness. Standard nonlinear least squares techniques were used to fit this relation to the multiaperture data for each object over the inner region of 16 kpc radius.

Profiles from three frames of the brightest galaxy in A 2197, along with the averaged fit to these data are illustrated in figure 3. This particular object is one of the most sharply cut off with increasing radius in the sample, and is less well fit than average. Lumpy profiles, such as that of A 21 are also relatively poorly fit. Fits to repeated observations made on the same night agree to 10% in core radius and $0\overset{m}{.}10$ in μ_c. A later paper in this series will undertake detailed investigation of the profiles of the galaxies in this sample, extending the results to large radii and faint surface brightness. The complete profiles will be published therein.

Although the observations were made under relatively good atmospheric conditions, with the more distant objects measured in the best seeing, the core radius and central surface brightness data are degraded by the atmosphere, telescope and detector (at least for the SIT). To correct for this, all suitably bright stars were located on the pictures and multiaperture photometry obtained as above. Gaussian fits to these data provided knowledge of the run of

image quality throughout each night. On average the image size was σ(= FWHM/2.35) = 0.7 arcsec and ranged from 0.3 to 1.0 arcsec.

Corrections to β and μ_c were estimated by synthesizing seeing degraded artificial galaxy profiles. Gaussians were numerically convolved with equation 1 over the full range of observed parameters σ and β. Multiaperture magnitudes were created from the profiles and the fit with the same procedure used for the actual observations. A large table was interpolated in for β(true) and $\Delta\mu_c$ given σ and β (observed). Core radius corrections averaged less than 25%, with $\Delta\mu_c$ generally less than $0\overset{m}{.}30$. Twelve galaxies spanning the full range of core radii were observed on more than one night under differing atmospheric conditions. Comparison of the corrected core radii shows an rms scatter of 13% with a $0\overset{m}{.}18$ scatter in μ_c. We adopt these values as the typical observational errors in these quantities. While this correction procedure is by no means optimal, it does not degrade the results of the present data appreciably.

Averaged corrected core radii from all frames of each object are listed in Table 1. Also listed are the average corrected central surface brightnesses. The final quantity in Table 1 is central surface brightness corrected for the galactic obscuration (as in Paper I) and corrected for the color change as a function of redshift, estimated from high quality multichannel spectrometer data. The change with redshift in pass-band width in the galaxies' rest frames,

normally included in the K-correction, has not been applied to the data in Table 1; this effect will be accounted for below.

III. RESULTS

Observational data now available for the 108 brightest cluster galaxies include the core radius and central surface brightness from Table 1 and absolute magnitude, redshift, and the cluster properties of richness and Bautz-Morgan type (BM) from Table 1 of Paper I. In order to compare the properties of various galaxies and explore relationships between these properties we must eliminate the effects of the redshift and establish "absolute" quantities for each galaxy. A Hubble constant of H_o = 60 km s^{-1} Mpc^{-1} and q_o = 1/2 are assumed throughout what follows. Each physical radius a corresponding to the galaxy core radius β listed in Table 2 is derived from

$$a(\text{kpc}) = 48.48 \frac{[1-(1+z)^{-\frac{1}{2}}]}{1+z} \beta(\text{arcsec}) \quad . \qquad (4)$$

The mean core radius from these data is $\langle a \rangle = 2.23 \pm 0.1$ kpc with a dispersion of σ_a = 1.09 kpc. Recalling that the observational uncertainty is 13% for this quantity, we find that this observed scatter is primarily cosmic.

A more convenient dimensionless parametrization of galaxy size is the power alpha used for the aperture cor-

rection by Gunn and Oke 1975 (hereafter GO), i.e.,

$$L = L_s(\gamma/\gamma_s)^{\alpha} . \tag{5}$$

We term α the structure parameter in what follows. Rewriting this expression as

$$\alpha = \left.\frac{d\ \ell n\ L}{d\ \ell n\ \gamma}\right]_{\gamma_s} \tag{6}$$

we find from equation (2)

$$\alpha = \frac{2\gamma_s^{\,2}}{(1+\gamma_s^{\,2}/\beta^2)\ \beta^2\ \ell n\ (1+\gamma_s^{\,2}/\beta^2)} \tag{7}$$

where γ_s is our sampling radius corresponding to 16 kpc. Column 4 of Table 2 is a list of α values which are histogrammed in figure 4. The mean of this distribution is $\langle\alpha\rangle = 0.49\pm0.01$ with a dispersion of $\sigma_\alpha = 0.11$. Observational uncertainties in β propagate to ±0.03 in α.

The final intrinsic parameter listed in Table 2 is the reduced surface brightness (RSB), which is the corrected central surface brightness of Table 1 further corrected for the fourth power redshift dimming appropriate for any relativistic cosmology (Hubble and Tolman 1935). A histogram of the RSB data appears as figure 5. The mean value is $\langle RSB\rangle = 18\overset{m}{.}13\pm0.06$ with a cosmic scatter of $\sigma_{RSB} = 0\overset{m}{.}62$.

These "mean galaxy" parameters are summarized in Table 3.

A result of Paper I (and earlier work; see, e.g., Kristian, Sandage, Westphal 1978) is that the absolute magnitudes of first-ranked galaxies are correlated with the cluster properties of richness and BM type. We find that the brightest galaxy structure is also correlated with these properties. In figure 6 the structure parameter histogram is subdivided by Abell richness class. Mean values for each class are given in Table 4. Although the sample suffers from a lack of rich clusters, an increase in the mean alpha of 0.06 per class is shown by the data. A weak correlation between structure parameter and cluster BM type is shown in figure 7. Means for each class are listed in Table 5. These correlations provide observational support for the dynamical friction galaxy evolution model in which the BM sequence is interpreted as a result of differing degrees of evolution with the Type I clusters being highly evolved. The structure parameter increases in this model as the cannibal dines on its neighbors and grows in luminosity at their expense, which happens at a faster rate in richer, denser systems (see GT or HO).

This dynamical evolution introduces important errors into the global Hubble diagram method of deceleration measurement. As stressed by GT, the aperture magnitudes of galaxies change with time, an effect which must be calibrated before meaningful results for q_o may be obtained. Another serious problem is that selection procedures tend

to find mainly rich, dense clusters at the faintest levels, and this correlation of galaxy and cluster properties introduces the well-known Scott (1957) effect. Is there any way of eliminating these problems? One possibility suggested by HO is the expected correlation of structure and absolute magnitude. Absolute intrinsic magnitudes from Table 2 are plotted against alpha in figure 8. The observational uncertainties are shown in the lower right. Evolutionary tracks in this plane are calculated by HO. The data are replotted in figure 9 where the points are average value in bins of 0.05 for alpha less than 0.5, and bins of 0.10 for alpha in excess of 0.5. The error bars represent $\pm 1\sigma$ dispersions in the data, where the uncertainty in the mean value is illustrated at the lower right. The dispersion of the data about the mean line is $\sigma = 0.22$ mag, and it decreases somewhat from left to right, consistent with the prediction of HO. This observed scatter is somewhat less than anticipated by HO.

In order to study this process in more detail, let us assume, following GT, that in a merger the galaxy scale size (a) increases as the kth power of the mass (m), that is if

$$\frac{\delta a}{a} = k \frac{\delta m}{m} \tag{8}$$

then

$$\frac{\delta L}{L} = \frac{\delta m}{m} (1-k\alpha) \tag{9}$$

if the accreted material has the same mass-to-light ratio as the original (GT equation 17). Taking $\chi = \beta/\gamma_s$, we derive

$$\frac{\delta L}{L} = \left(\frac{1}{k} - \alpha\right) \frac{\delta \chi}{\chi} \tag{10}$$

which may be integrated to obtain

$$L_s = c' \chi^{1/k} \ell n (1+1/\chi^2) \tag{11}$$

or

$$M_s = -2.5 \log [\chi^{1/k} \ell n(1+1/\chi^2)] + c . \tag{12}$$

This relation, along with equation (7) may be used to find the expected behavior in the (M_{VI}, α) plane for various k. Two such loci are shown in figure 9 for k = 1 and k = 2, having been vertically adjusted to fit the data at $\alpha = 0.49$. The case k = 1 is the expected behavior (GT) for the homologous merger of galaxies of nearly the same size, whereas k = 2 is expected for large objects consuming small ones. The data are remarkably well fit by the k = 1 case. HO have suggested relatively large objects located near the cannibal to be its most likely victims, which is consistent with this observed behavior and the large luminosity difference between the first and second ranked galaxies in highly evolved (BMI) systems (Sandage and Hardy 1973).

Absolute magnitudes and structure parameters are plotted

as functions of cluster redshift in figure 10. A trend in the data towards larger, more luminous galaxies with increasing distance in the sample is apparent. This effect is too large to be easily explained by incorrect choice of q_o (a value 6σ away from the formal result of Paper 1 is necessary to explain the data). An alternate hypothesis is that a selection effect exists in the distance class limited sample. Atypical clusters containing larger, more luminous brightest galaxies than average are included in the sample, particularly at the largest redshifts beyond the completeness limit ($z \sim 0.06$) of the sample. Applying a statistical correction to the absolute magnitudes based on the measured values of alpha for each galaxy and the mean line defined by the data in figure 9 eliminates this dependence of absolute magnitude on redshift. It appears that this "α-correction" may be used to correct for the effects of selection bias in cluster samples and thereby eliminate the Scott effect

During the course of obtaining the redshifts for the clusters in this sample it was noticed that a sizeable fraction of the first-ranked galaxies have multiple nuclei. This is not apparent on Schmidt prints (or plates) due to excessive density and insufficient scale. A small subset of these objects are the binary objects studied by Rood and Leir (1979). In order to determine the fraction of multiple systems and isolate individuals for further study, a photographic survey of the sample on short exposure large-scale plates was undertaken with the 2.5-meter Hooker and the

1.5-meter Palomar telescopes. Halfway through this project the SIT system became available and was used to complete the survey. One well-known multiple system, in A 2199, is shown in figure 1. All galaxies in the sample with multiple components separated by less than 16 kpc are listed in Table 6. Two of these clusters, A 88 and A 1656 are not included in the discussion below for lack of sufficient surface photometry. Two objects, in A 2199 and A 21, are triple systems. Thirty-three sample galaxies are multiple - a fraction of 28%. A sizeable number of such systems is expected to form during dynamical evolution (GT, HO). The mean absolute magnitude of the multiple systems is $\langle M_{VI} \rangle = -22.76$, while $\langle M_{VI} \rangle = -22.64$ for the remainder. The mean structure parameter for the multiple galaxies is $\langle \alpha \rangle = 0.53$ with $\langle \alpha \rangle = 0.48$ for the rest. The ratio of these changes, $\Delta M/\Delta\alpha$, is nearly equal to the slope of the mean (M_{VI} -α) relation of figure 9 near $\alpha = 0.49$, indicating that the presence of the extra components does not strongly affect the derivation of the structure parameter. If we assume that these changes of 0.12 mag and 0.05 in α are typical for the accretion of a galaxy, we can crudely estimate that the "average" sample galaxy was formerly four smaller ones; from both the magnitude and alpha differences of the "mean" galaxy and the faintest, smallest observed first-ranked galaxies with $\alpha = 0.30$ and $M_{VI} = -22.15$, which are identified with the primordial state. The time since cluster collapse for the average sample cluster is somewhat less than 5×10^9 years (the

appropriate value for the Coma Cluster, Gunn and Gott 1972). On average, then, a cluster member is consumed about once every 10^9 years, which is in agreement with the typical relaxation time for a massive galaxy in the central region of a rich cluster (Bahcall 1977). If all mergers result in a detectable multiple system at some stage, we can estimate a lifetime of about 2.5×10^8 years, which agrees well with current theoretical merger timescale estimates of about an orbital time.

One more observed relationship supports the dynamical evolution model. Reduced surface brightness and structure parameters are plotted in figure 11. Typical observational error is also shown. The dispersion of the RSB data about the mean relation defined by the data is $\sigma = 0\overset{m}{.}23$; approximately half of the variance can be accounted for by the observational uncertainties. For the simple homologous merger of N objects to form a giant (i.e., the k = 1 case above) the central surface brightness is expected to decrease like 1/N (see OH). The "average" sample galaxy has RSB = $18\overset{m}{.}13$, which is a factor of four down from the RSB of the smallest, least luminous galaxies in the sample. This result provides independent confirmation that approximately four objects have on average merged to create the first-ranked galaxy. To summarize, the observational results discussed in this section are all entirely consistent with dynamical merger of galaxies in clusters. The high frequency of multiple nucleus systems is difficult to explain

without such evolution.

IV. DISCUSSION

This evolution of the brightness and structure of brightest galaxies has important consequences for observational cosmology, particularly its influence on the values of the deceleration obtained from global methods. Is the alpha correction all that is necessary to eliminate this systematic effect, or are the corrected magnitudes still correlated with other properties, such as cluster richness or BM type? Alpha-corrected absolute magnitudes are histogrammed by richness class in figure 12. Mean absolute magnitudes for each class are listed in Table 7. The clear trend towards brighter galaxies in richer clusters, shown in figure 2 of Paper I for these data, has all but disappeared. Corrected magnitudes binned by BM type are shown in figure 13, and the mean values tabulated in Table 8. Again the trend found in Paper I has been eliminated. Richness plus BM corrections for each galaxy are plotted against the alpha correction in figure 14. We believe the alpha correction, which reduces the dispersion in the magnitudes of first-ranked galaxies to $\sigma = 0.21$ mag, is the more fundamental method, richness and BM magnitude trends being due to correlation of galaxy structure with these cluster properties. The results shown in figure 14 suggest that the richness and BM corrections cannot properly eliminate the evolution, particularly for nearly primordial

(i.e., $\alpha \sim 0.3$) objects. Work in progress will determine if other cluster properties, such as the form of the luminosity function or the central number density of galaxies may be used in place of the alpha correction (see HO).

For faint high-redshift clusters the quantity alpha is not impossible to measure (since 16 kpc corresponds to 2.5 arcsec at $z = 0.6$), but it will not be easy. Also, in order to measure alpha q_o must be known. An iterative procedure may be used to solve for q_o with the Hubble diagram; alpha corrections calculated for some initial q_o are applied and a new q_o derived, then the procedure is repeated until it converges. Since intrinsically brighter galaxies are larger and an incorrect value of q_o results in an error of the same sign, i.e., too large a q_o corresponds to brighter, larger angular size galaxies, the alpha correction reduces the sensitivity of the Hubble diagram to q_o. This reduction in sensitivity is of the same order as the gains from the reduced dispersion the correction provides. If some property of the cluster, independent of q_o, can be found to correlate well with the evolutionary state of the brightest galaxy, this sensitivity reduction may be avoided.

If we ignore selection bias in the data used at present for the Hubble diagram (fig. 4 of Paper I) we can estimate the influence of dynamical evolution on that result. The time between the epoch of the faint clusters ($z \sim 0.3$) and the epoch of the bright clusters ($z \sim 0.07$) corresponds to consumption of two or three galaxies by the cannibal. At

Δ = 0.12 mag per event a correction to the formal value of q_o in the range $1 < \Delta q_o < 1.7$ in the sense q_o (true) = q_o (formal) + Δq_o is necessary. A similar correction of opposite sign is the best available estimate for the influence of the evolution of the stellar populations in the galaxies (Tinsley and Gunn 1976, hereafter cited as TG). Thus the true deceleration is probably near the formal value, in the absence of selection bias in the sample used.

Clusters richer on average than the low redshift sample are preferentially selected at large distances; thus the dynamical evolutionary correction is somewhat offset by selection. A quantitative estimate of the magnitude of this effect cannot yet be made.

The deviation from the $1/(1+z)^4$ behavior of central surface brightness with redshift has been proposed as a means of measuring the rate of stellar evolution in galaxies (Gudehus 1975, Petrosian 1976, Tinsley 1976). The large dispersion introduced by dynamical evolution of the central surface brightness, as well as the systematic trend with redshift and selection bias, combine to render raw central surface brightness useless for this purpose. Measurement of the structure parameter may be used to eliminate these problems, via the relationship shown in figure 11, with the price that the surface brightness-redshift effect is no longer independent of cosmological model. Alpha-corrected central surface brightness is plotted as a function of log (1+z) in figure 15. The scatter in the data is large,

but a correlation does exist with a best fit slope of 13.7 $\pm$2.8, slightly over 1σ from the expected slope of 10 for no evolution. It has long been realized that this plot can provide a fundamental direct test for the expansion of the universe (Hubble and Tolman 1935, Geller and Peebles 1972). Tired light cosmologies, where the change in energy per photon with redshift is the only effect, have a slope in this plane of 2.5, which is 4σ from the observations.

Assuming the absence of strong radial gradients, the stellar evolution of central surface brightness is (following GO)

$$\delta SB = (1.3-0.3x)\ \ell n\ t_1/t_o \qquad (13)$$

where x is defined for the stellar mass (m_s) function in a galaxy by

$$\frac{dN}{dm_s} = C\ m_s^{-(1+x)} \qquad (14)$$

For $q_o = 1/2$ (where $t_1/t_0 = \frac{1}{(1+z)^{3/2}}$) and x = 1 (see TG) we list expected δSB's for several redshifts in Table 9. The slope error for the data in figure 15 corresponds to $0\overset{m}{.}10$ at z = 0.07 where most of our data are. Thus the data lie 2σ away from the expected line, including evolution. Improved measurements can make sizeable improvements in the significance of this sort of result, since half the slope error may be attributed to the present observational

uncertainties. Careful extension of these data to larger distances is necessary before actual estimates of the evolution rate may be obtained. If the slope of the surface brightness-redshift relation continues to exceed 10, the extra complication of intergalactic extinction may have to be faced (Gudehus 1975).

An alternate global test using galaxies is the metric diameter-redshift relation. Baum (1972) has applied this method using a clever photographic technique. Others have suggested core radii for first-ranked galaxies to be good metric rods, independent of the stellar evolution (Petrosian 1976, Tinsley 1976). A core radius-redshift plot for our data is shown in figure 16, along with the expected behavior for $q_o = 0$ and $q_o = 1$. (See e.g. Sandage 1961 for theory.) The separation between these models amounts to 30% at $z = 0.6$. The cosmic dispersion in core radii is $\sim$50% which, along with the systematic dynamical evolution of the core radii, makes this method less than attractive. Also faint cluster samples are biased towards larger galaxies, as discussed in Section III.

The correlation between core radius and central surface brightness may be used to reduce this dispersion and eliminate the systematic trends, but the rate of stellar population evolution must be known before these corrections can be applied. The core radius - RSB relation is shown in figure 17. Elimination of the systematic trend reduces the observed core radius dispersion to $\sigma_a = 22\%$; half of

this variance corresponds to the observational uncertainties. Accurate rates for the stellar evolution of central surface brightness are necessary before the β-z diagram becomes a viable method. From the ground, the core radius measurements for high redshift clusters are difficult at best, but the Space Telescope will have sufficient sensitivity and resolution to measure directly both the core radius and central surface brightness at any redshift.

Resolving the entanglement of deceleration and evolution will be difficult if only magnitudes, core radii, central surface brightnesses and redshifts are available. Incorrect estimation of the stellar evolution rates results in q_o error of the same sign for both the Hubble diagram and metric diameter tests. The magnitude of the errors is, however, not identical for the two methods; only the correct stellar evolution rate should result in the same deceleration being determined from both techniques. It remains to be seen whether all other systematic effects can be eliminated to the extent that this becomes practical.

The mean surface brightness-core radius relation defined by the data shown in figure 17 may be written as

$$RSB = 2.93 \log a + 17.15. \qquad (15)$$

This is identical to the relation found by Kormendy (1977) (after accounting for photometric system differences and the definition of core radius), largely from King's (1978)

photometry of Virgo Cluster ellipticals of considerably lower absolute luminosity than the present sample. Acceptance of the evolutionary cause for this relation for the first-ranked galaxies hints that a physically similar process, i.e., the homologous merger of small systems to form larger ones, may be important in the formation of all elliptical galaxies. Accurate surface photometry of a large sample of galaxies extending deep into the cluster luminosity function to check this result is necessary, and could provide an important clue for the detailed understanding of the galaxy formation process.

V. SUMMARY

Surface photometric observations of the brightest galaxies in 108 Abell clusters lead to several conclusions relevant to observational cosmology.

1) All available evidence indicates that dynamical friction strongly affects the structure and luminosity of first-ranked galaxies.

2) Galaxy structure is correlated with the cluster properties of richness and Bautz-Morgan effects.

3) Galaxy absolute magnitude is correlated with structure. An observed relation may be used to eliminate the dependence of absolute magnitude on cluster properties, minimize the dispersion in magnitude to $\sigma = 0.21$ mag, and remove the systematic trend of dynamical evolution.

4) The average nearby Abell cluster has had four members combine to form the giant which grows in aperture luminosity by 0.12 mag for each capture, which happens with a timescale of $\sim 10^9$ years.

5) This rate implies a correction in the range $1<\Delta q_o<1.7$ is necessary for the Hubble diagram method. Stellar evolution requires a correction of similar size and opposite sign; the true q_o should thus not be far from the formal value.

6) Surface brightnesses, corrected for the effects of dynamical evolution, follow the behavior with redshift expected for relativistic cosmologies. Improved observations may allow measurement of the rate of evolution of the

stellar population in galaxies.

7) Galaxy core radii are strongly modified by dynamical effects, but correction for these influences is possible. Such data might be a viable subject for a metric diameter-redshift test, which can provide a useful complement to the Hubble diagram and aid in the elimination of systematic bias in the final results for the deceleration parameter.

TABLE 1

Observational Data

Abell	β (arcsec)	μ_c (mu)	$\mu_c(A,K)$ (mu)	Abell	β (arcsec)	μ_c (mu)	$\mu_c(A,K)$ (mu)	Abell	β (arcsec)	μ_c (mu)	$\mu_c(A,K)$ (mu)	Abell	β (arcsec)	μ_c (mu)	$\mu_c(A,K)$ (mu)
21...	3.47	19.69	19.35	978...	1.14	17.84	17.65	1651...	1.63	19.06	18.88	2079...	1.73	18.56	18.42
76...	1.57	18.90	18.82	1020...	0.91	17.87	17.73	1691...	1.75	18.86	18.71	2092...	1.43	18.91	18.77
85...	5.72	19.99	19.87	1035...	1.18	18.46	18.29	1749...	1.27	17.96	17.84	2107...	2.95	18.88	18.79
104...	2.54	19.87	19.59	1126...	2.11	19.14	18.96	1767...	1.23	18.33	18.18	2124...	1.60	18.79	18.65
119...	2.20	18.58	18.48	1139...	1.21	17.89	17.81	1773...	1.28	18.51	18.34	2142...	1.69	19.62	19.42
147...	2.04	18.86	18.77	1185...	4.03	18.94	18.87	1775...	1.05	17.97	17.82	2147...	2.49	18.60	18.47
151...	2.06	18.31	18.20	1187...	1.38	18.61	18.44	1793...	0.90	18.59	18.41	2151...	2.20	18.26	18.13
154...	1.33	18.16	17.99	1213...	1.05	17.55	17.45	1795...	2.04	18.94	18.80	2152...	1.28	17.92	17.78
166...	0.94	19.51	19.26	1216...	0.97	18.03	17.92	1809...	1.33	18.42	18.25	2162...	1.51	17.48	17.37
168...	1.55	18.19	18.09	1228...	1.01	17.43	17.36	1831...	1.52	18.58	18.42	2175...	1.39	19.06	18.80
189...	1.24	17.58	17.51	1238...	0.97	18.28	18.12	1904...	1.35	18.24	18.09	2197...	2.10	17.38	17.26
193...	1.62	17.66	17.56	1254...	1.16	18.33	18.15	1913...	1.38	18.70	18.59	2199...	4.57	18.66	18.53
194...	1.60	16.92	16.88	1291...	1.67	19.25	19.12	1927...	1.85	19.51	19.35	2255...	0.99	18.07	17.78
225...	1.38	18.68	18.46	1318...	1.41	16.89	16.85	1983...	0.85	17.67	17.57	2256...	2.51	18.50	18.20
246...	0.94	18.40	18.25	1364...	0.92	18.71	18.48	1991...	2.23	19.04	18.91	2328...	0.98	19.11	18.67
274...	1.21	19.25	18.98	1365...	1.12	18.44	18.28	1999...	1.82	19.47	19.25	2347...	1.16	19.25	18.94
277...	1.22	18.92	18.72	1367...	1.99	17.30	17.26	2005...	1.54	19.60	19.33	2382...	1.98	19.29	19.15
389...	2.01	19.79	19.54	1377...	0.94	17.57	17.46	2022...	1.43	18.24	18.12	2384...	1.93	19.70	19.50
399...	2.64	19.87	19.62	1382...	1.58	19.25	18.98	2028...	1.12	18.24	18.07	2399...	0.69	17.49	17.31
400...	0.97	16.60	16.55	1399...	1.16	19.06	18.86	2029...	2.94	19.09	18.92	2410...	1.49	18.90	18.73
401...	1.71	19.03	18.77	1412...	2.12	19.92	19.69	2040...	1.13	18.15	18.05	2457...	1.67	18.36	18.23
496...	2.64	18.31	18.11	1436...	1.22	18.35	18.21	2048...	1.29	18.47	18.27	2634...	1.99	17.85	17.62
500...	1.18	18.27	18.03	1468...	1.05	18.77	18.59	2052...	2.87	18.90	18.82	2657...	1.98	19.26	19.17
634...	2.31	18.26	17.94	1474...	1.05	18.96	18.79	2061...	1.25	18.20	18.03	2666...	2.16	17.58	17.37
671...	2.00	18.33	18.07	1496...	1.27	19.54	19.33	2063...	2.75	18.83	18.76	2670...	1.16	18.15	17.99
779...	2.31	17.33	17.24	1541...	1.16	18.62	18.43	2065...	1.77	19.17	19.02	2675...	1.49	18.88	18.72
957...	1.65	18.03	17.87	1644...	2.68	19.02	18.88	2067...	0.99	18.67	18.51	2700...	1.32	18.99	18.78

TABLE 2

Intrinsic Properties of Galaxies

Abell	M_{VI}	a(kpc)	α	RSB(mu)	Abell	M_{VI}	a(kpc)	α	RSB(mu)	Abell	M_{VI}	a(kpc)	α	RSB(mu)
21...	-23.30	6.80	0.90	18.94	1228...	-22.14	0.76	0.33	17.22	2028...	-22.92	1.84	0.45	17.75
76...	-22.61	1.34	0.40	18.66	1238...	-22.49	1.49	0.42	17.82	2029...	-23.43	4.86	0.74	18.60
85...	-22.98	7.01	0.92	19.64	1254...	-22.49	1.59	0.43	17.88	2040...	-22.07	1.16	0.38	17.86
104...	-22.76	4.41	0.70	19.25	1291...	-21.97	2.15	0.49	18.88	2048...	-22.94	2.52	0.52	17.88
119...	-22.71	2.20	0.49	18.29	1318...	-21.96	0.63	0.31	16.77	2052...	-22.50	2.30	0.50	18.67
147...	-22.23	2.02	0.47	18.59	1364...	-22.71	2.00	0.47	18.04	2061...	-23.09	2.08	0.48	17.71
151...	-23.15	2.40	0.51	17.97	1365...	-22.58	1.82	0.45	17.96	2063...	-22.45	2.12	0.48	18.61
154...	-23.01	1.78	0.45	17.73	1367...	-22.38	0.95	0.35	17.17	2065...	-22.59	2.74	0.55	18.71
166...	-22.28	2.17	0.49	18.79	1377...	-22.52	1.06	0.37	17.25	2067...	-22.23	1.54	0.42	18.21
168...	-22.54	1.59	0.43	17.90	1382...	-22.86	3.37	0.61	18.54	2079...	-22.97	2.46	0.52	18.14
189...	-22.05	0.99	0.36	17.36	1399...	-22.37	2.20	0.49	18.48	2092...	-22.31	2.07	0.48	18.49
193...	-22.84	1.73	0.44	17.35	1412...	-22.39	3.74	0.64	19.34	2107...	-22.84	2.80	0.55	18.61
194...	-22.83	0.67	0.31	16.81	1436...	-22.73	1.71	0.44	17.94	2124...	-22.87	2.32	0.50	18.36
225...	-22.69	2.06	0.48	18.17	1468...	-22.50	1.88	0.46	18.23	2142...	-22.46	3.20	0.59	19.05
246...	-22.18	1.51	0.42	17.93	1474...	-22.11	1.74	0.44	18.47	2147...	-22.59	2.13	0.49	18.31
274...	-22.97	3.04	0.58	18.45	1496...	-22.37	2.52	0.52	18.94	2151...	-22.55	1.80	0.45	17.98
277...	-22.85	2.39	0.51	18.32	1541...	-22.81	2.16	0.49	18.06	2152...	-22.45	1.27	0.39	17.59
389...	-22.95	4.66	0.72	19.06	1644...	-22.55	2.74	0.55	18.69	2162...	-22.55	1.10	0.37	17.24
399...	-22.66	4.10	0.67	19.32	1651...	-22.87	2.89	0.56	18.53	2175...	-22.74	2.80	0.55	18.40
400...	-22.16	0.52	0.29	16.45	1691...	-22.94	2.71	0.54	18.40	2197...	-23.08	1.46	0.41	17.13
401...	-22.82	2.75	0.55	18.45	1749...	-22.86	1.57	0.43	17.60	2199...	-23.25	3.28	0.60	18.40
496...	-22.71	1.97	0.47	17.97	1767...	-22.86	1.88	0.46	17.88	2255...	-22.92	1.58	0.36	17.47
500...	-22.74	1.70	0.44	17.75	1773...	-22.91	2.11	0.48	18.02	2256...	-23.30	3.05	0.58	17.97
634...	-22.35	1.42	0.41	17.93	1775...	-22.88	1.62	0.43	17.52	2328...	-23.37	2.65	0.54	18.10
671...	-23.10	2.21	0.49	17.86	1793...	-22.51	1.61	0.43	18.05	2347...	-22.73	2.76	0.55	18.45
779...	-22.92	1.09	0.37	17.15	1795...	-22.79	2.80	0.55	18.54	2382...	-22.37	2.79	0.55	18.88
957...	-22.91	1.62	0.43	17.68	1809...	-23.12	2.22	0.49	17.92	2384...	-22.51	3.77	0.64	19.11
978...	-22.73	1.33	0.40	17.42	1831...	-23.04	2.43	0.52	18.11	2399...	-22.38	0.89	0.34	17.07
1020...	-22.16	1.28	0.39	17.46	1904...	-23.12	2.08	0.48	17.78	2410...	-22.88	2.54	0.53	18.39
1035...	-22.88	2.00	0.47	17.95	1913...	-22.33	1.63	0.43	18.36	2457...	-22.86	2.18	0.49	17.98
1126...	-23.16	3.68	0.64	18.62	1927...	-22.36	2.93	0.56	19.04	2634...	-22.91	1.44	0.41	17.49
1139...	-22.14	1.03	0.36	17.65	1983...	-21.99	0.87	0.34	17.38	2657...	-21.68	1.85	0.46	19.00
1185...	-22.80	3.21	0.59	18.72	1991...	-22.64	2.88	0.56	18.67	2666...	-23.11	1.36	0.40	17.25
1187...	-22.38	2.32	0.59	18.11	1999...	-22.84	3.83	0.65	18.82	2670...	-23.00	1.91	0.46	17.68
1213...	-22.69	1.13	0.38	17.24	2005...	-22.91	3.80	0.65	18.82	2675...	-22.61	2.32	0.50	18.42
1216...	-22.18	1.13	0.38	17.70	2022...	-22.62	1.78	0.45	17.88	2700...	-22.86	2.66	0.54	18.38

TABLE 3

Summary of Mean Galaxy Properties

Quantity	Mean	σ
M_{VI} ...	-22.68 ± 0.03 mag	0.35
log $a_{..}$	0.30	0.20
α	0.49 ± 0.01	0.11
RSB ...	$18^{m}.13$ ± 0.06	0.62

TABLE 4

Mean Structure Parameter by Richness Class

Richness	$< \alpha >$	σ
0...	0.41 ± 0.02	0.06
1...	0.49 ± 0.01	0.11
2...	0.54 ± 0.03	0.11
3...	0.52	

TABLE 5

Mean Structure Parameter by Bautz-Morgan Type

B-M	$< \alpha >$	σ
I.....	0.59 ± 0.05	0.17
I-II....	0.52 ± 0.03	0.09
II.....	0.50 ± 0.02	0.10
II-III...	0.47 ± 0.02	0.11
III.....	0.47 ± 0.01	0.07

TABLE 6

Clusters with Multiple Component Brightest Galaxies

Abell	Abell	Abell
21	779	2067
88	1126	2092
104	1185	2142
151	1291	2151
154	1468	2175
193	1496	2199
194	1656	2256
277	1927	2328
389	1991	2384
400	2052	2410
671	2063	2634

TABLE 7

Mean Absolute Magnitudes after Alpha-Correction

Richness	$< M_{VI}(\alpha) >$	σ
0...	-22.80 ± 0.13	0.40
1...	-22.63 ± 0.03	0.28
2...	-22.75 ± 0.08	0.33
3...	-22.88	

TABLE 8

Mean Absolute Magnitudes after Alpha-Correction

BM	$< M_{VI}(\alpha) >$	σ
I.....	-22.79 ± 0.07	0.24
I-II....	-22.76 ± 0.10	0.31
II.....	-22.75 ± 0.07	0.28
II-III..	-22.70 ± 0.06	0.30
III.....	-22.56 ± 0.05	0.30

TABLE 9

Stellar Evolutionary Surface Brightness

Changes for X=1

z	δSB (mu)
0.07...	0.10
0.15...	0.21
0.30...	0.39
0.60...	0.70

REFERENCES

Bahcall, N. A. 1977, Ann. Rev. Astr. Ap., 15, 505.

Baum, W. A. 1972, in External Galaxies and Quasi Stellar Objects, ed. Evans, IAU, 393.

Dressler, A. 1978a, Ap. J., 222, 23.

———— 1978b, Ap. J., 223, 765.

———— 1979, Ap. J., 231, 659.

Geller, M. J. and Peebles, P. J. E. 1972, Ap. J., 174, 1.

Gudehus, D. H. 1975, PASP, 87, 763.

Gunn, J. E. and Gott, R. 1972, Ap. J., 176, 1.

Gunn, J. E. and Oke, J. B. 1975, Ap. J. 195, 255.

Gunn, J. E. and Tinsley, B. M. 1976, Ap. J., 210, 1.

Hausman, M. A. and Ostriker, J. P. 1978, Ap. J., 224, 320.

Hoessel, J. G., Gunn, J. E., and Thuan, T. X. 1980, in preparation.

Hubble, E. P. and Tolman, R. C. 1935, Ap. J., 82, 302.

Kent, S. M. 1979, PASP, 91, 394.

King, I. R. 1978, Ap. J., 222, 1.

Kormendy, J. 1977, Ap. J., 218, 333.

Kristian, J., Sandage, A., and Westphal, J. A. 1978, Ap. J., 221, 383.

Oemler, A. 1976, Ap. J., 209, 693.

Ostriker, J. P. and Tremaine, S. D. 1975, Ap. J. (Letters), 202, L113.

Ostriker, J. P. and Hausman, M. A. 1977, Ap. J. (Letters), 217, L125.

Petrosian, V. 1976, Ap. J. (Letters), 209, L9.

Rood, H. J. and Leir A. A. 1979, Ap. J. (Letters), 231, L3.

Sandage, A. 1961, Ap. J., 133, 355.

———————— 1972, Ap. J., 178, 1.

———————— 1976, Ap. J., 205, 6.

Sandage, A. and Hardy E. 1973, Ap. J., 183, 743.

Scott, E. L. 1957, A. J., 62, 248.

Thuan, T. X. and Gunn, J. E. 1976, PASP, 88, 543.

Tinsley, B. M. 1976, Ap. J. (Letters), 210, L49.

Tinsley, B. M. and Gunn, J. E. 1976, Ap. J., 203, 52.

White, S. D. M. 1976, MNRAS, 174, 19.

Young, P. J., Westphal, J. A., Kristian, J., Wilson, C. P., and Landauer F. P. 1978, Ap. J., 221, 721.

Figure 1

Dezeroed and flattened red frames of six galaxies from the sample. The picture of A 166 is a CCD frame obtained with the Hale telescope one arcminute on a side. The rest are SIT frames two arcminutes in size made with the 1.5-meter telescope. Frames of A 2124 and A 2029 have been digitally stretched for higher contrast.

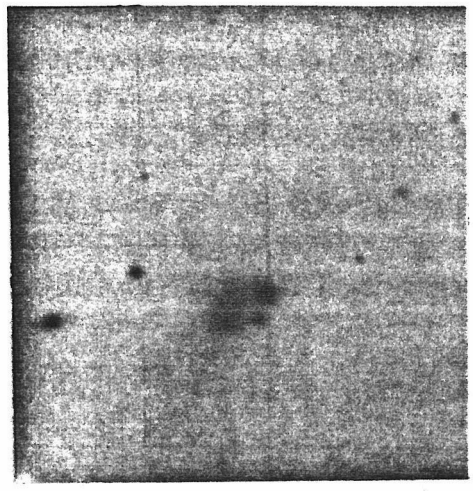

2199

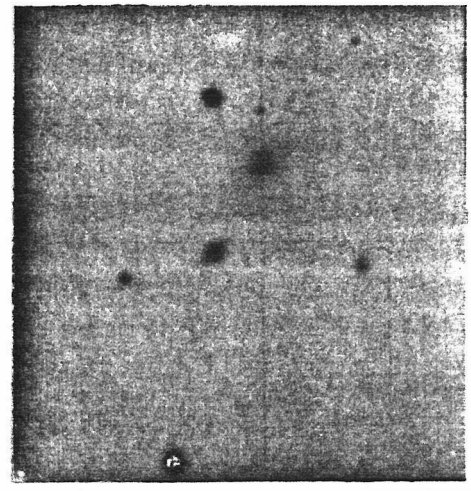

1795

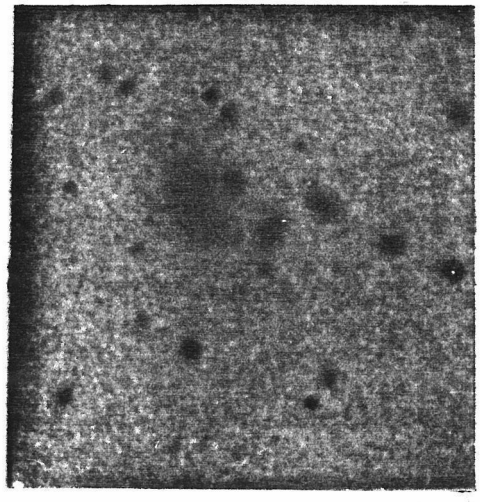

2124

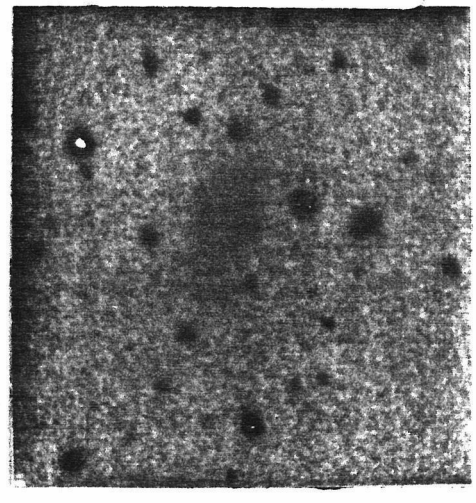

2029

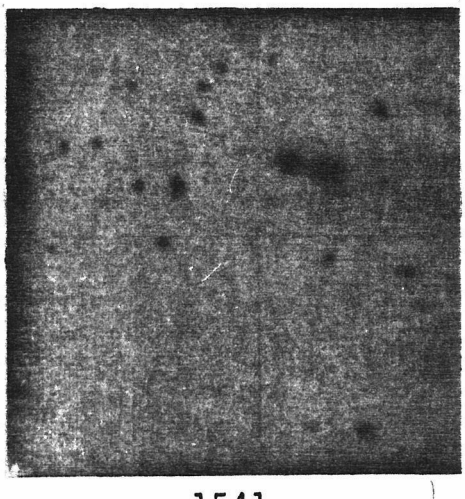

1541

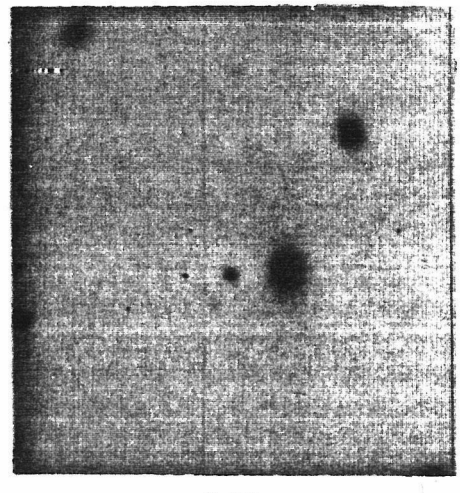

166

Figure 2

Red surface brightness (in units of mag arcsec^{-2}) profiles for six galaxies in the sample (γ is angular radius in arcseconds). These objects were chosen to exhibit the range of characteristics observed in the entire sample. Final profiles extending to faint surface brightness for the entire sample will be published elsewhere.

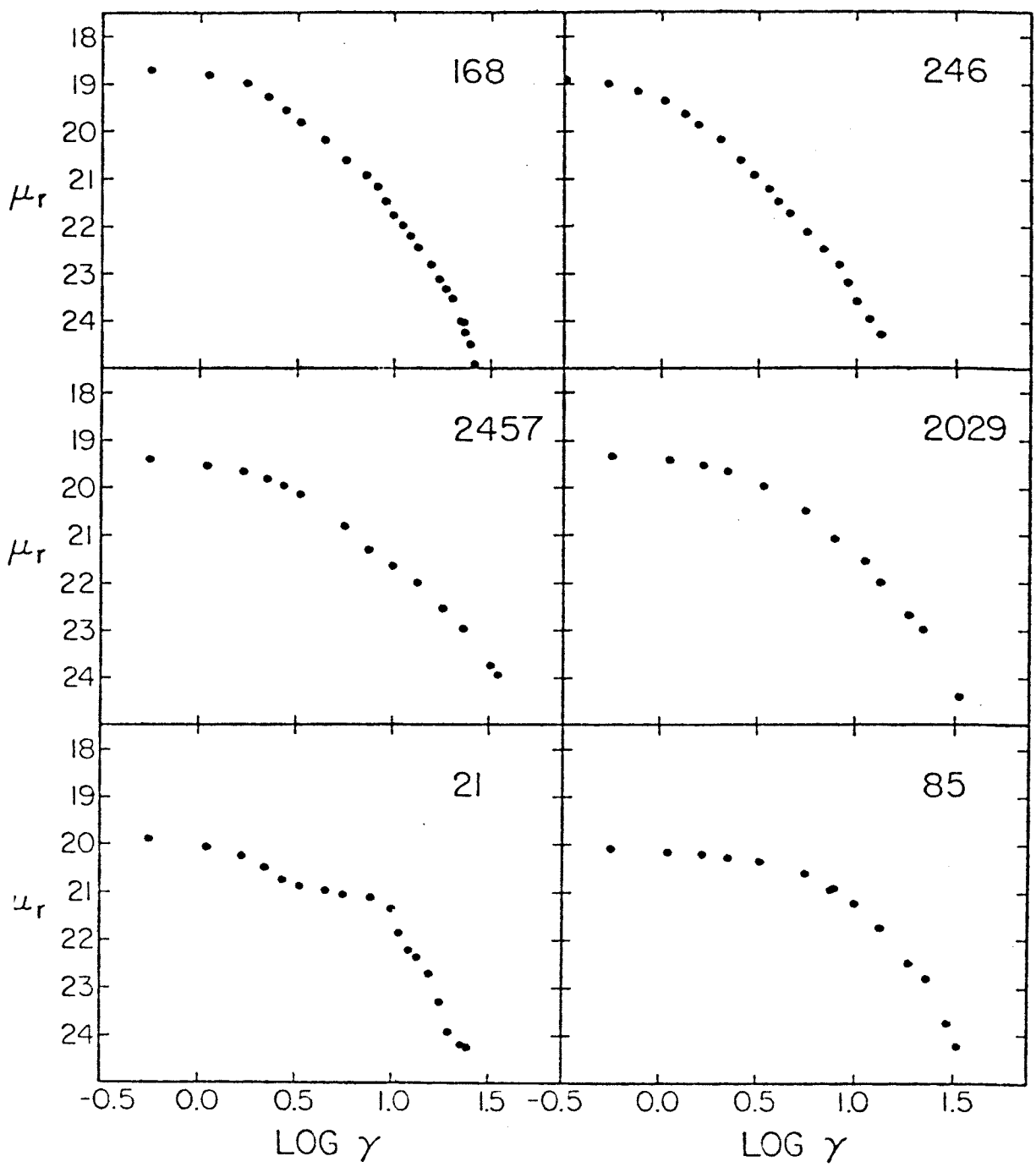
168
246
2457
2029
21
85
μ_r
μ_r
μ_r
18
19
20
21
22
23
24
-0.5
0.0
0.5
1.0
1.5
LOG γ
LOG γ

Figure 3

Average fit (solid line) to the observed profiles (points) for three red pictures of the brightest galaxy in A 2197. The fit extends to 16 kpc metric radius. This object is fit somewhat less well than average; it is one of the most strongly truncated with increasing radius in the sample.

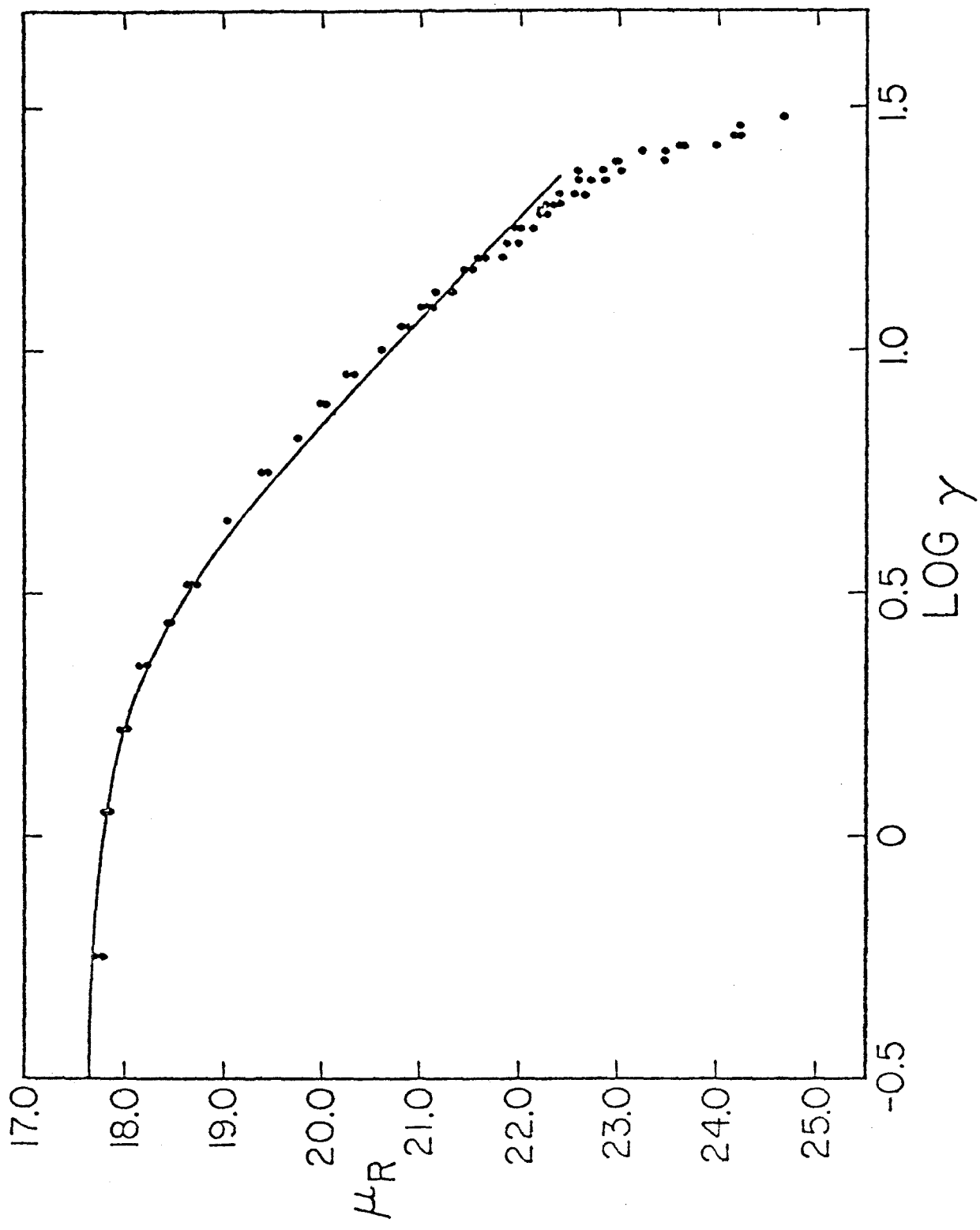
17.0
18.0
19.0
20.0
21.0
22.0
23.0
24.0
25.0
μ_R
-0.5
0
0.5
1.0
1.5
LOG γ

Figure 4

Histogram of the dimensionless structure parameters for the 108 galaxies in the sample. The mean of this distribution is $\langle\alpha\rangle = 0.49$ with the dispersion $\sigma_\alpha = 0.11$.

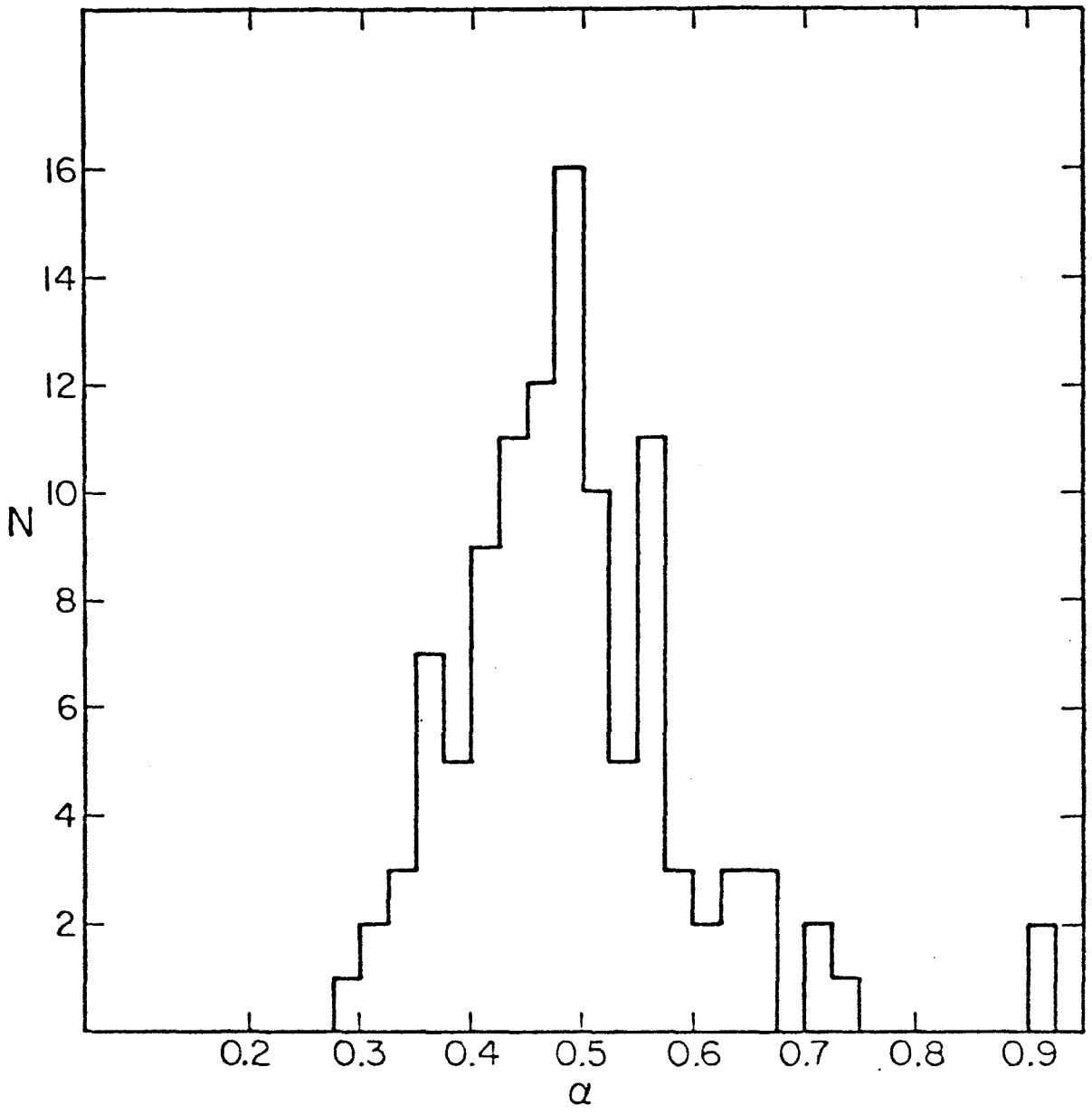
16
14
12
N 10
8
6
4
2
0.2
0.3
0.4
0.5
0.6
0.7
0.8
0.9
α

Figure 5

Histogram of reduced central surface brightness for the galaxies in the sample. The mean is $\langle RSB \rangle = 18^{m}.13$ with dispersion $\sigma_{RSB} = 0^{m}.62$.

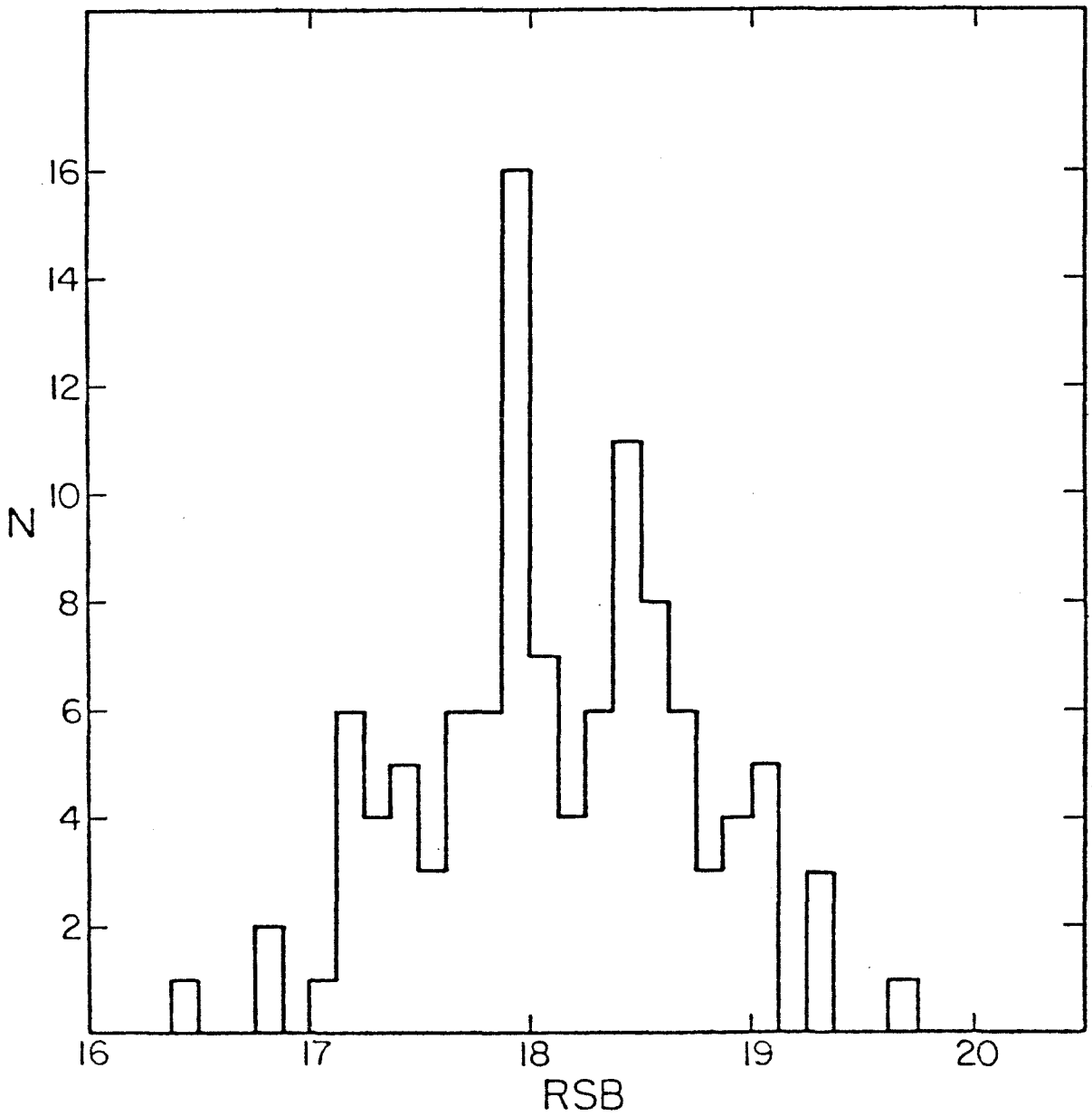
N
16
14
12
10
8
6
4
2
16
17
18
19
20
RSB

Figure 6

Histogram of structure parameter data for each Abell richness class. Mean alphas for each class are listed in Table 4.

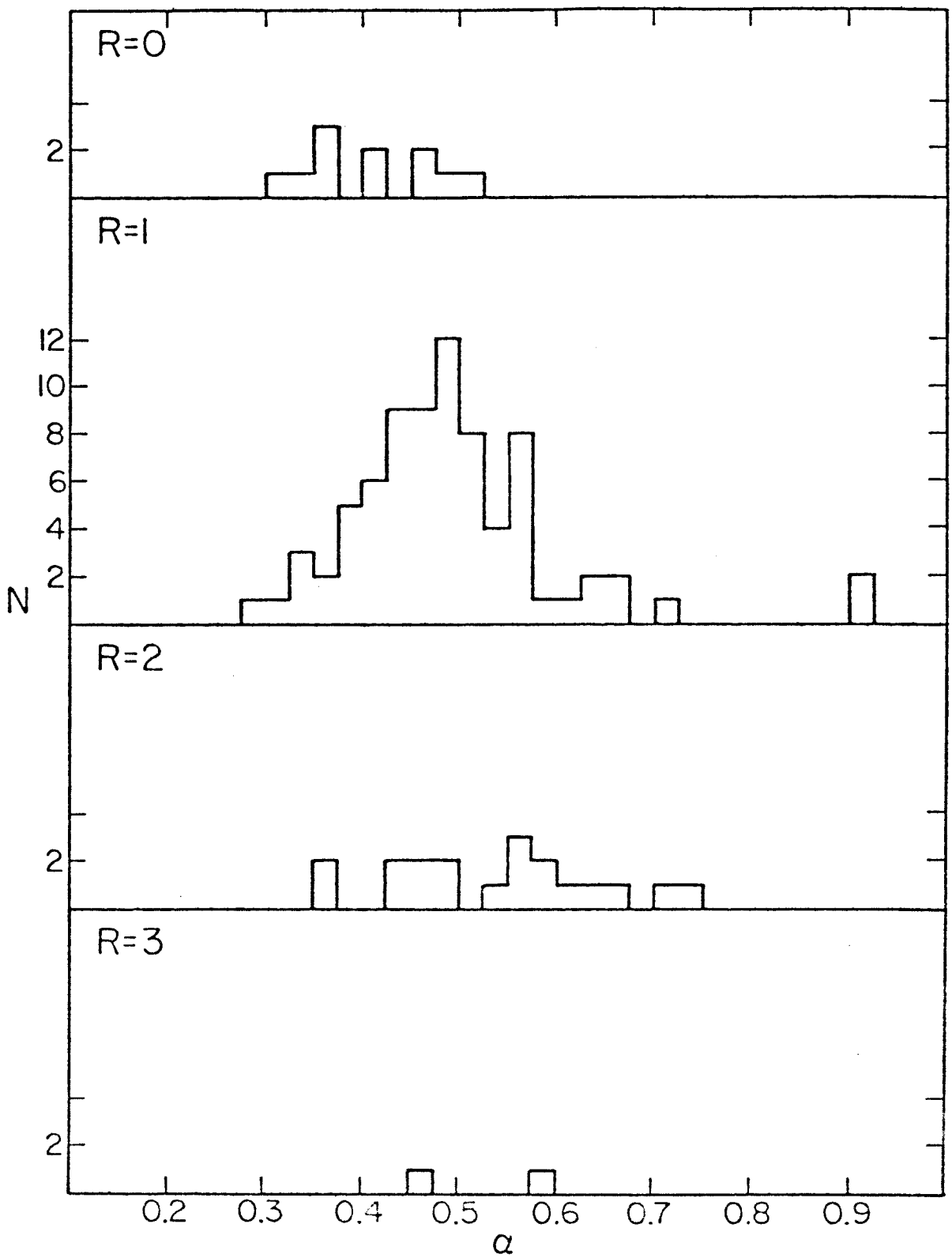
R=0
2
R=1
12
10
8
6
4
2
N
R=2
2
R=3
2
0.2
0.3
0.4
0.5
0.6
0.7
0.8
0.9
α

Figure 7

Histogram of structure class for each cluster Bautz-Morgan type. Mean alphas for each type are listed in Table 5.

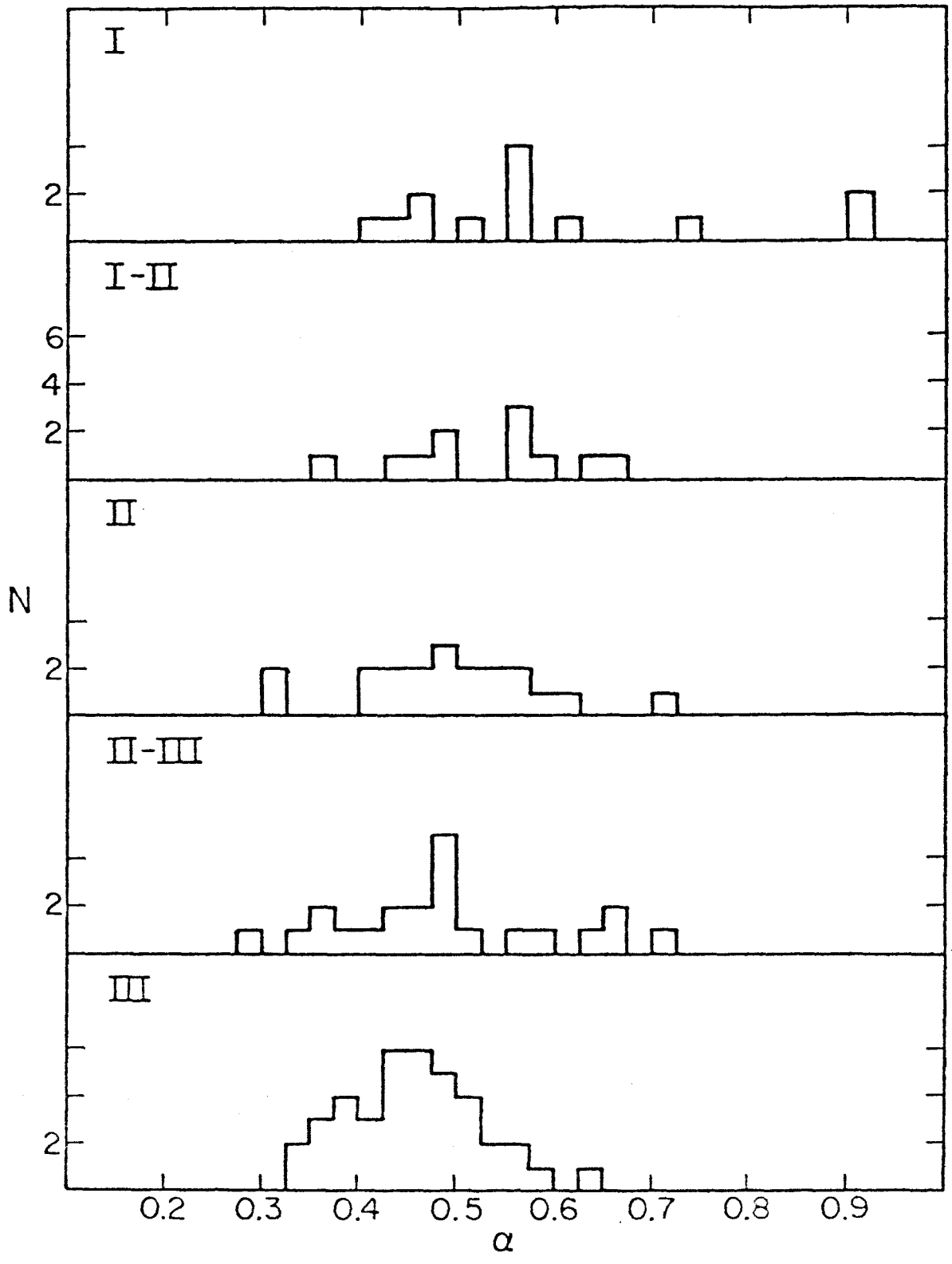
I
I-II
II
II-III
III
N
2
6
4
2
2
2
2
0.2
0.3
0.4
0.5
0.6
0.7
0.8
0.9
α

Figure 8

Absolute intrinsic magnitudes in a 16 kpc radius aperture are plotted against structure parameter for the sample galaxies. The error bars at the lower right illustrate the observational uncertainty in each point. An interesting comparison may be made between this figure (data) and figure 3 of Hausman and Ostriker (1978) (theory).

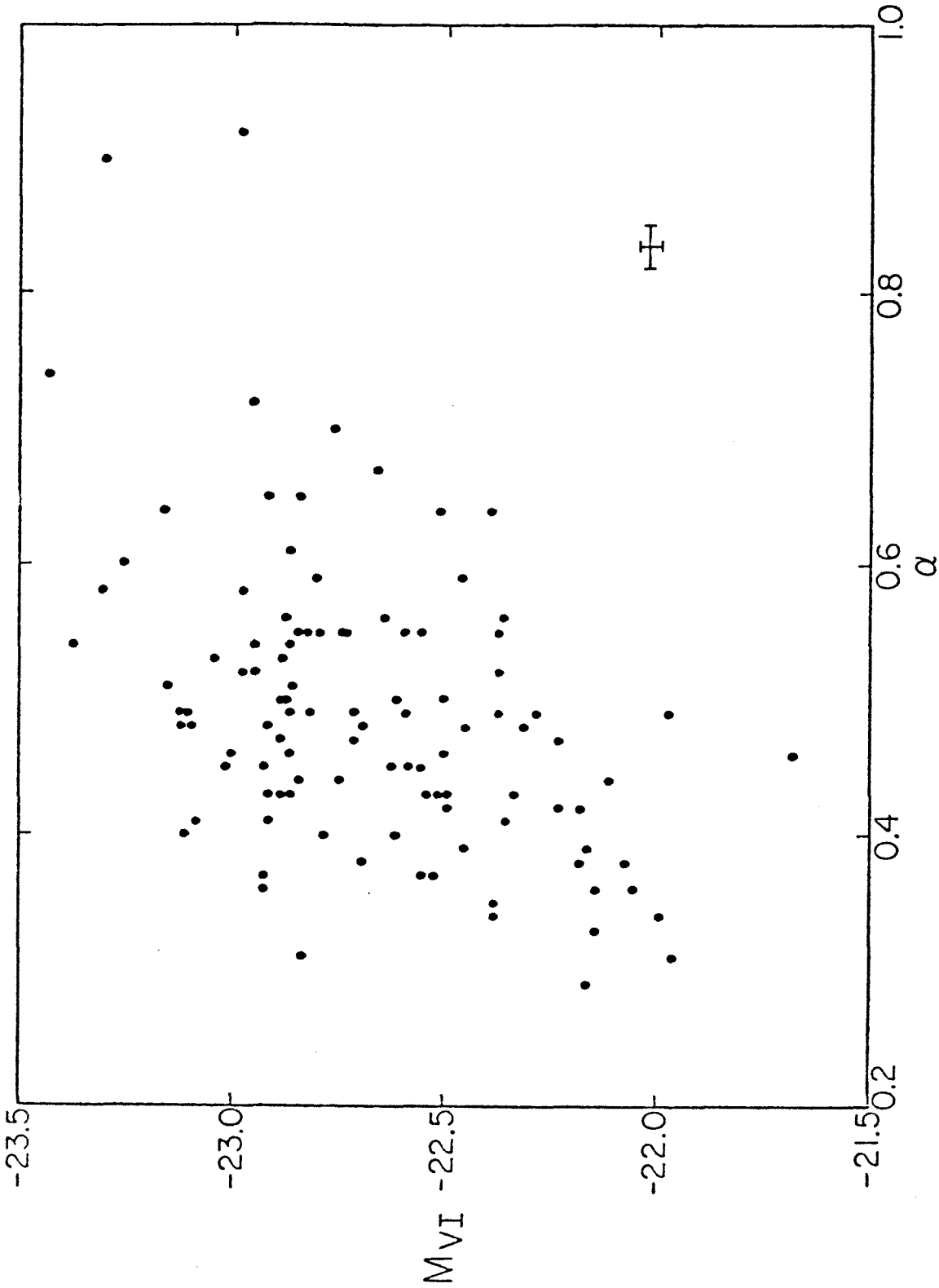
-23.5
-23.0
-22.5
-22.0
-21.5
M_{VI}
0.2
0.4
0.6
0.8
1.0
α

Figure 9

The data of figure 8 are replotted as mean absolute magnitudes in bins of structure parameter. The error bars represent the dispersions in the data. Errors in the determination of the mean points are shown at the lower right. As explained in the text the solid curves are the theoretically expected loci for two different rates of galaxy core growth with accreted mass.

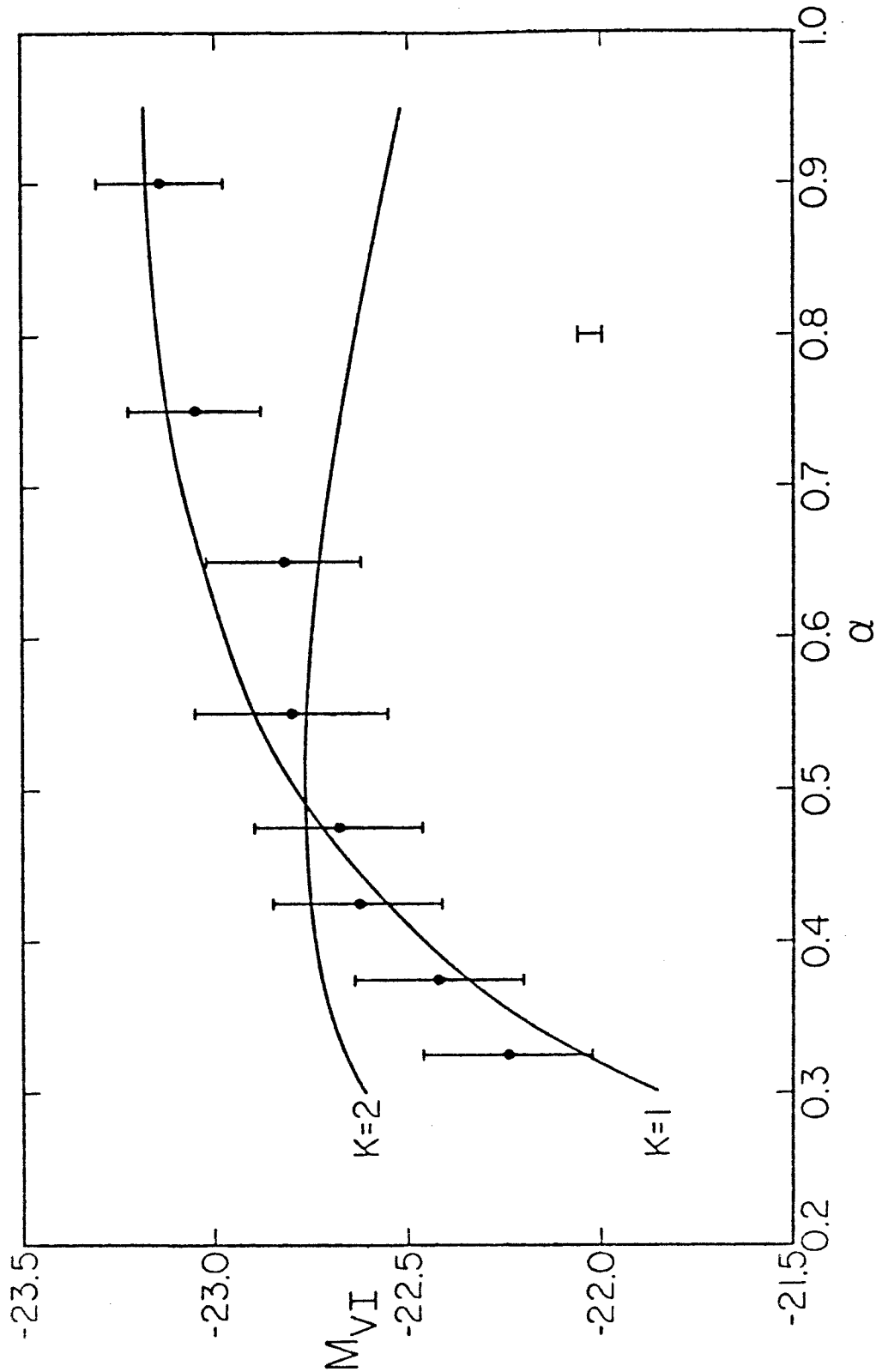
-23.5
-23.0
-22.5
-22.0
-21.5
M_{VI}
0.2
0.3
0.4
0.5
0.6
0.7
0.8
0.9
1.0
α
K=2
K=1
I

Figure 10

Correlations of intrinsic absolute magnitude (upper panel) and structure parameter (lower panel) with redshift for galaxies in the sample. Interpreted as selection bias in the distance class limited sample, the trend of increasing absolute brightness with redshift is eliminated if the data are corrected via the mean (M_{VI} - α) relation (shown in figure 9).

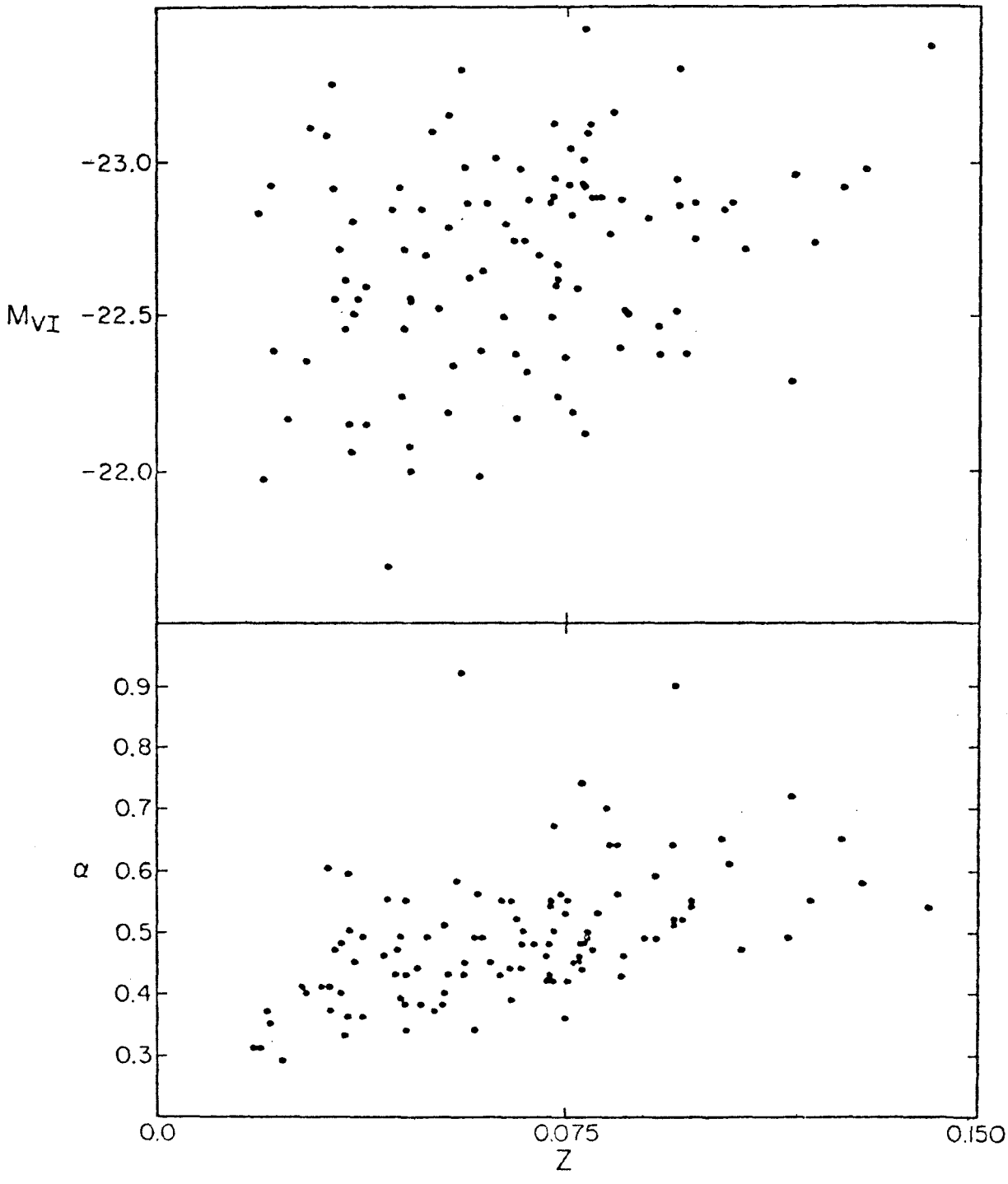
-23.0
-22.5
-22.0
M_{VI}
0.9
0.8
0.7
0.6
0.5
0.4
0.3
α
0.0
0.075
0.150
Z

Figure 11

Reduced central surface brightness is plotted as a function of galaxy structure parameter for the data (from Table 2). Observational uncertainties appropriate for each point are illustrated at the lower right. Dispersion of the surface brightness data about the mean RSB - α relation defined by the data is $\sigma = 0\overset{m}{.}23$.

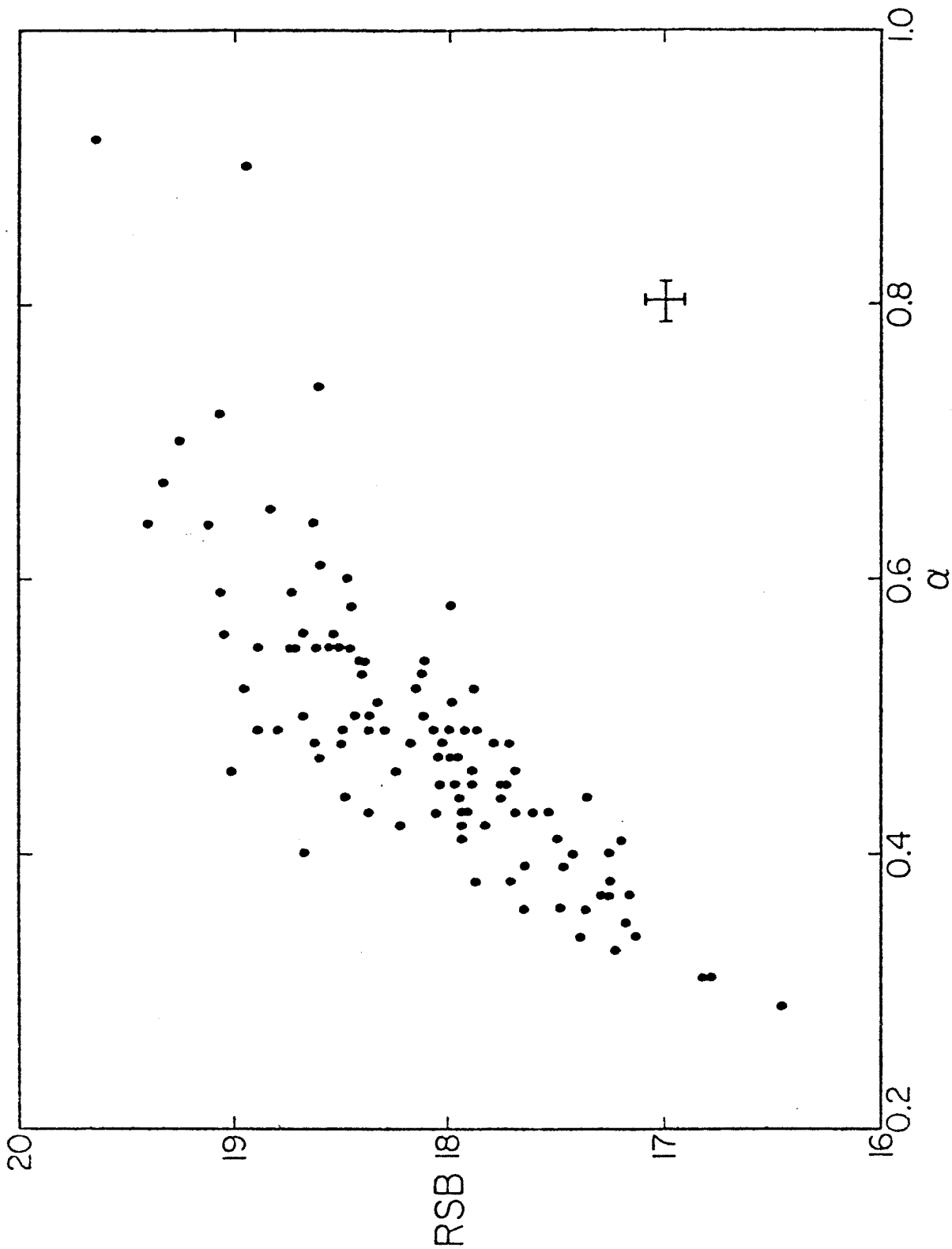
20
19
18
17
16
RSB
0.2
0.4
0.6
0.8
1.0
α

Figure 12

Alpha-corrected absolute magnitudes are histogrammed for each cluster richness class. The clear trend of brighter brightest galaxies in richer clusters (Paper I) has been eliminated by the alpha correction.

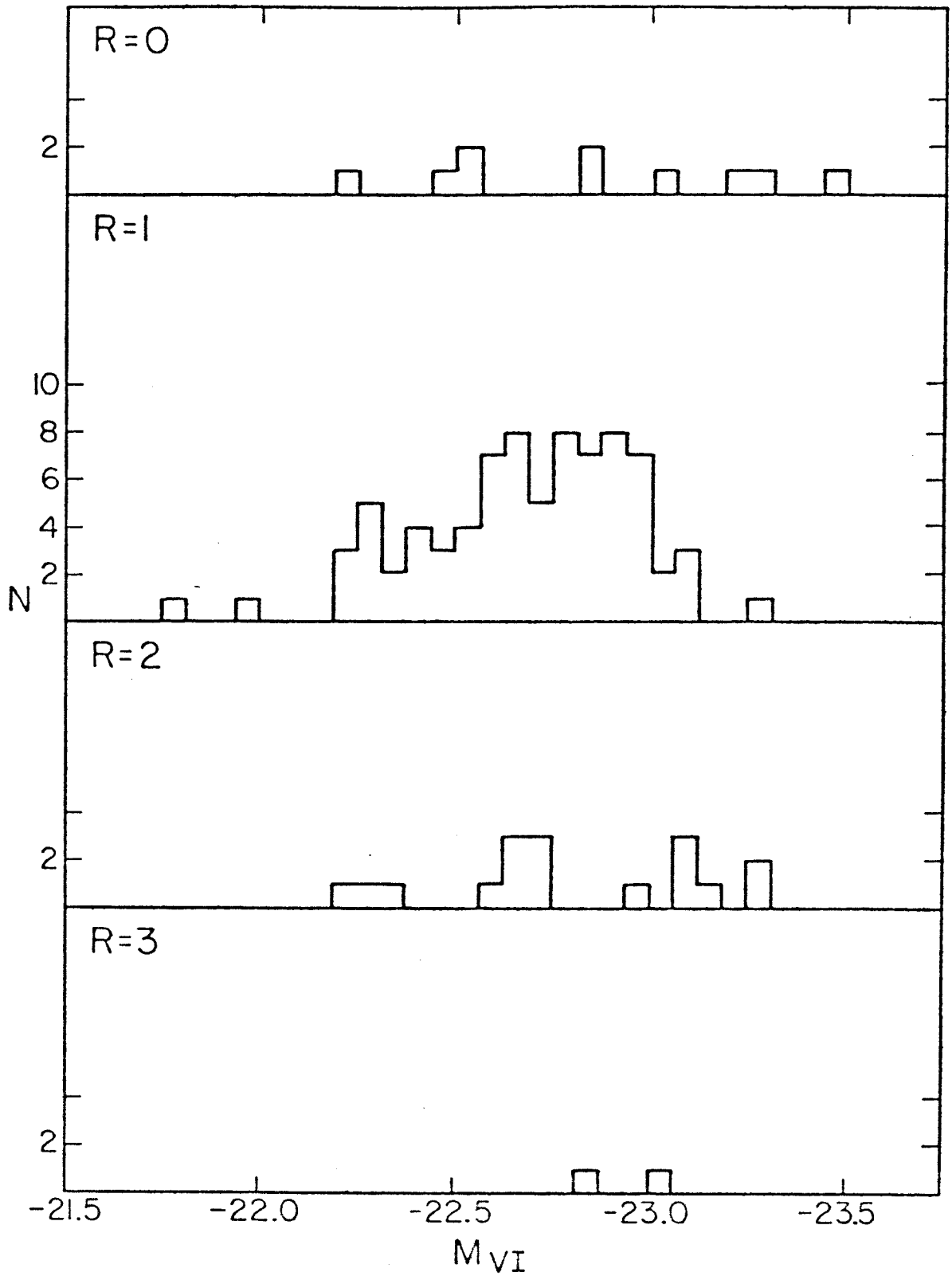
R=0
2
R=1
10
8
6
4
2
N
R=2
2
R=3
2
-21.5
-22.0
-22.5
-23.0
-23.5
M VI

Figure 13

Alpha-corrected absolute magnitudes are histogrammed for each cluster Bautz-Morgan type. The trend found in the uncorrected data shown in figure 3 of Paper I is reduced to less than statistically significant by the alpha correction.

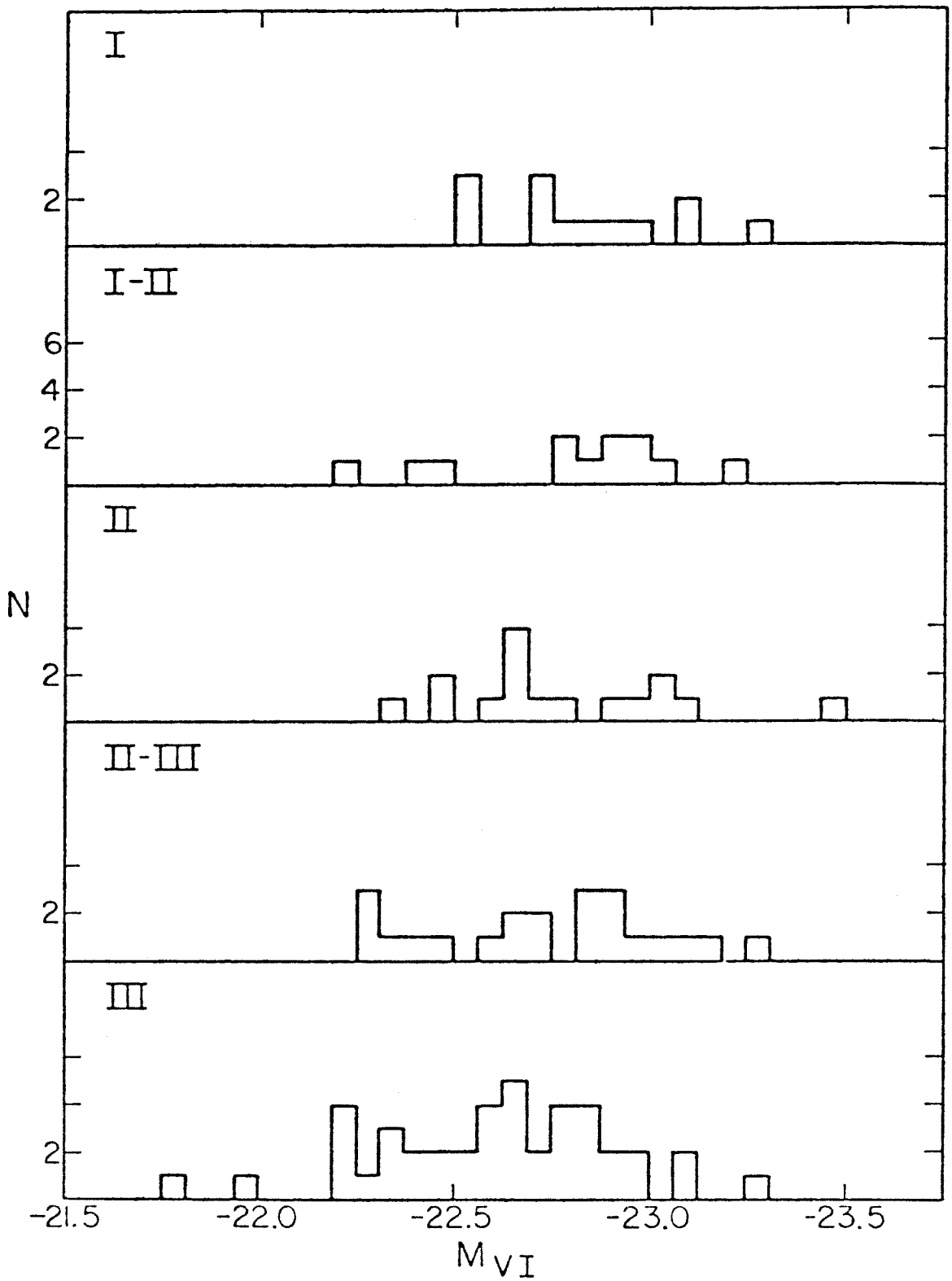
I
I-II
II
II-III
III
N
2
6
4
2
-21.5
-22.0
-22.5
-23.0
-23.5
M_{VI}

Figure 14

Richness plus Bautz-Morgan corrections derived from the data of Paper I are plotted against the alpha corrections for each galaxy in the sample. Perfect correlation is illustrated by the line. The $\Delta M(R+BM)$ appears to fail, particularly for systems with small (nearly primordial) core radii.

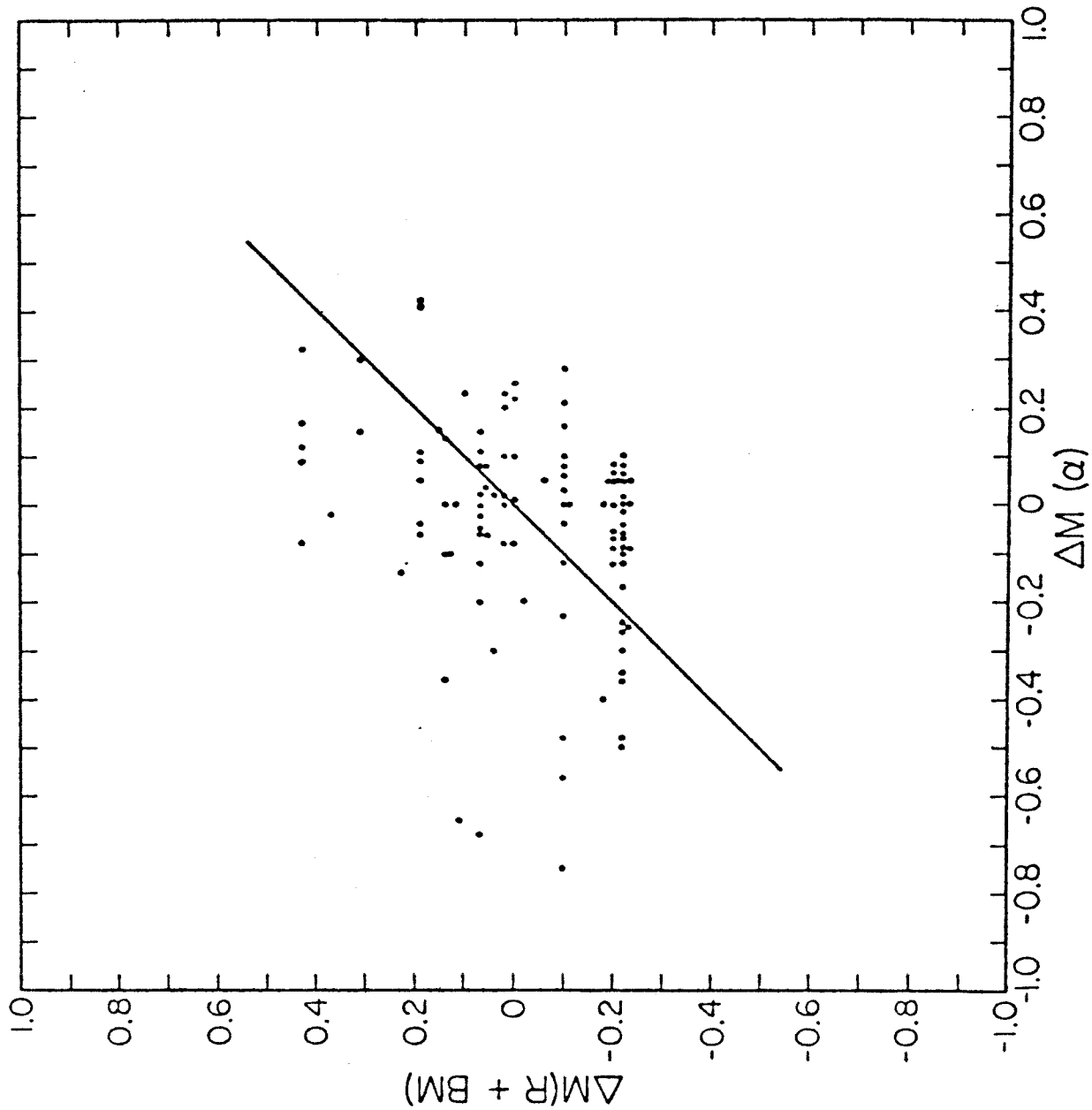
ΔM(R + BM)
ΔM (α)
1.0
0.8
0.6
0.4
0.2
0
-0.2
-0.4
-0.6
-0.8
-1.0
-1.0
-0.8
-0.6
-0.4
-0.2
0
0.2
0.4
0.6
0.8
1.0

Figure 15

Totally corrected central surface brightness is plotted as a function of log (1+z). The best fit line has a slope of 13.7 $\pm$ 2.8. In the absence of stellar evolution a slope of 10 is expected for all relativistic cosmologies. Tired light universes (slope 2.5) are inconsistent with these data.

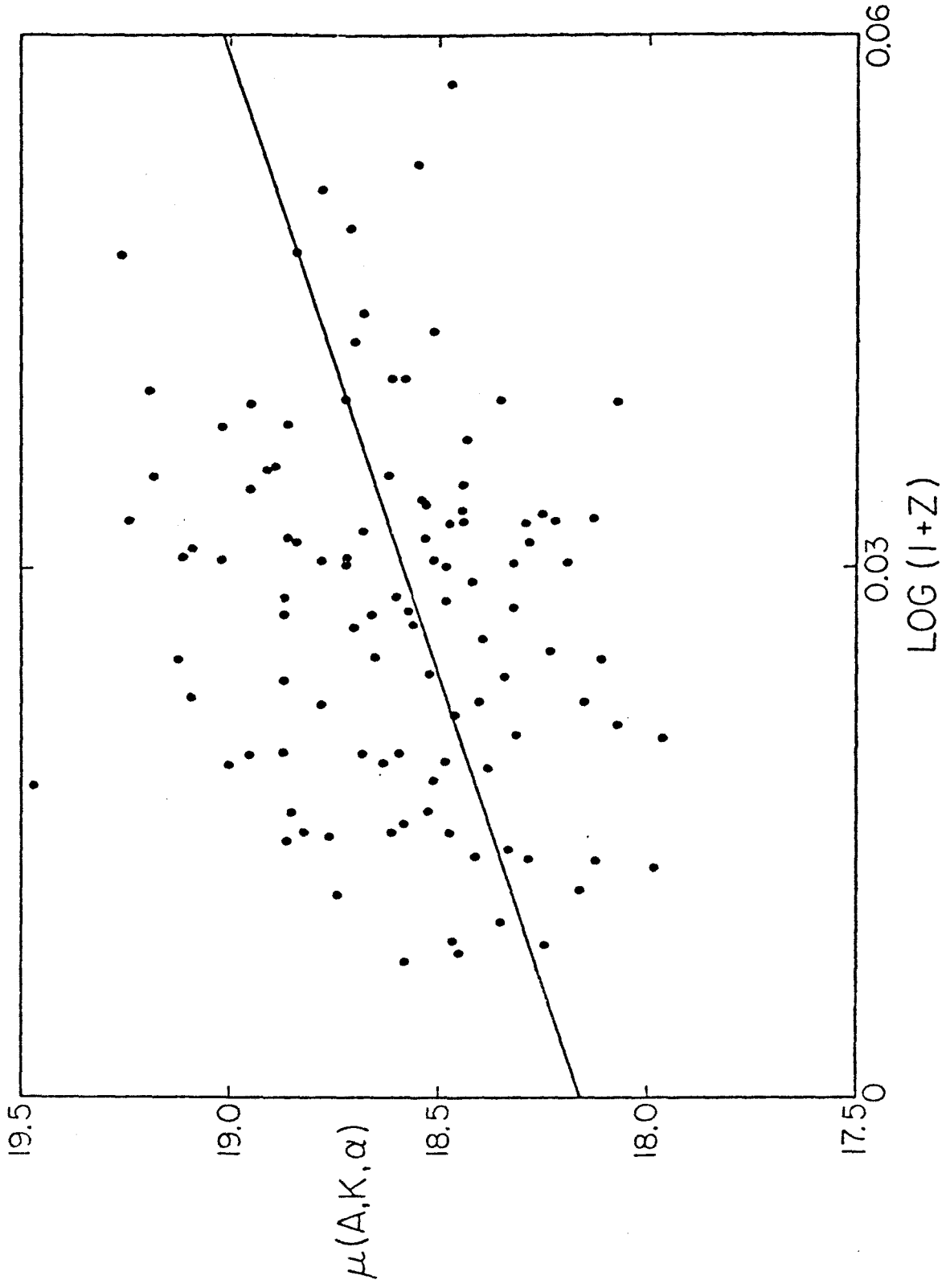
19.5
19.0
18.5
18.0
17.5
μ(A,K,α)
0
0.03
0.06
LOG (1+Z)

Figure 16

The core radius-redshift diagram has been proposed as a cosmological test. The large dispersion and systematic bias in raw core radius data for any cluster sample combine to make this method less than promising. Core radii, corrected by their correlation with central surface brightness, are a much superior statistic, but the method is then no longer independent of the evolution of the stellar population in these galaxies.

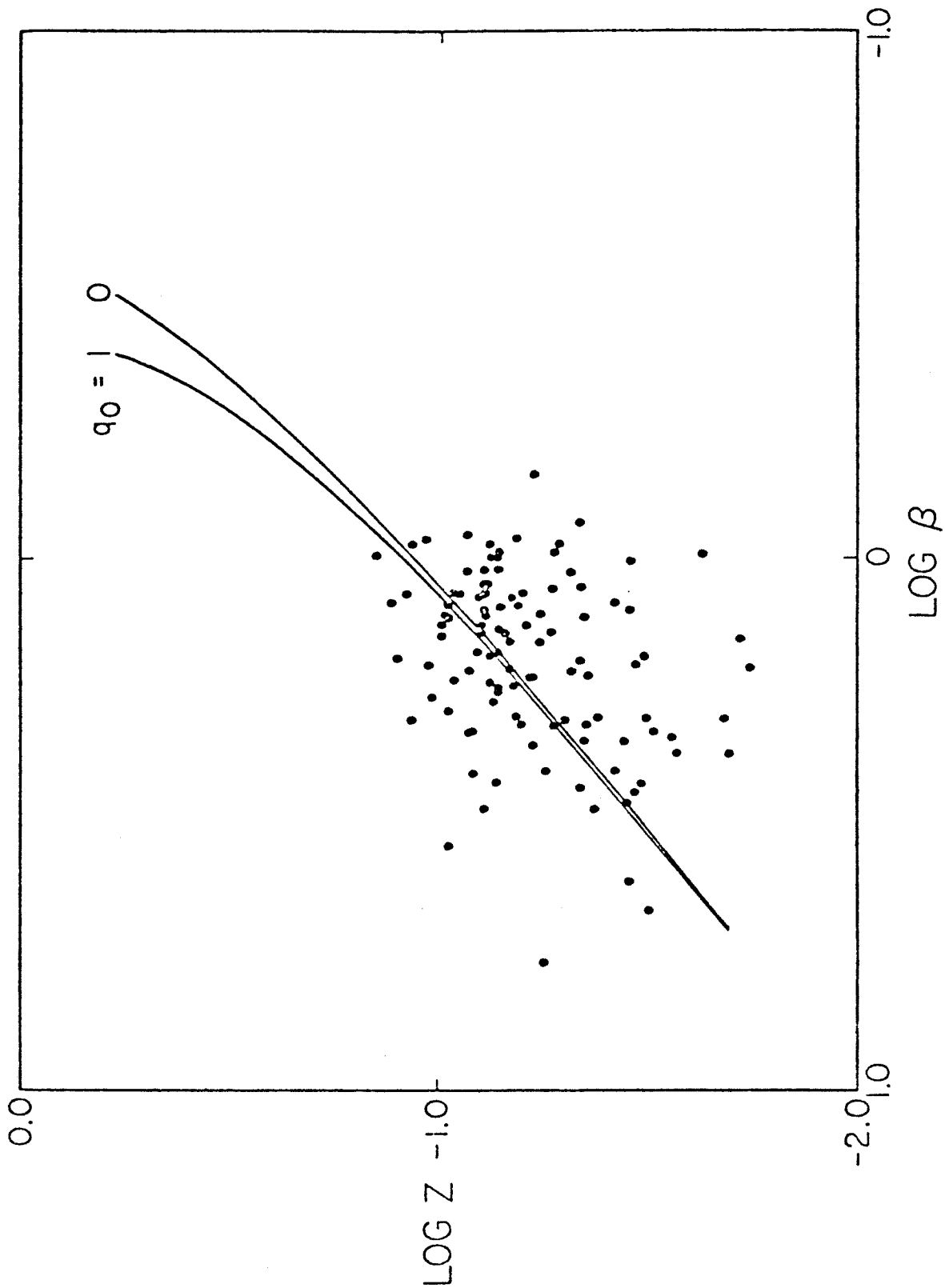
0.0
-1.0
-2.0
LOG Z
-1.0
0
-1.0
LOG β
$q_0 = 1$
0

Figure 17

Galaxy core radii are plotted against central surface brightness. A relation of the form RSB = 2.93 log a +17.15 fits the data well. This relation also holds for lower absolute luminosity ellipticals in the Virgo cluster (Kormendy 1977).

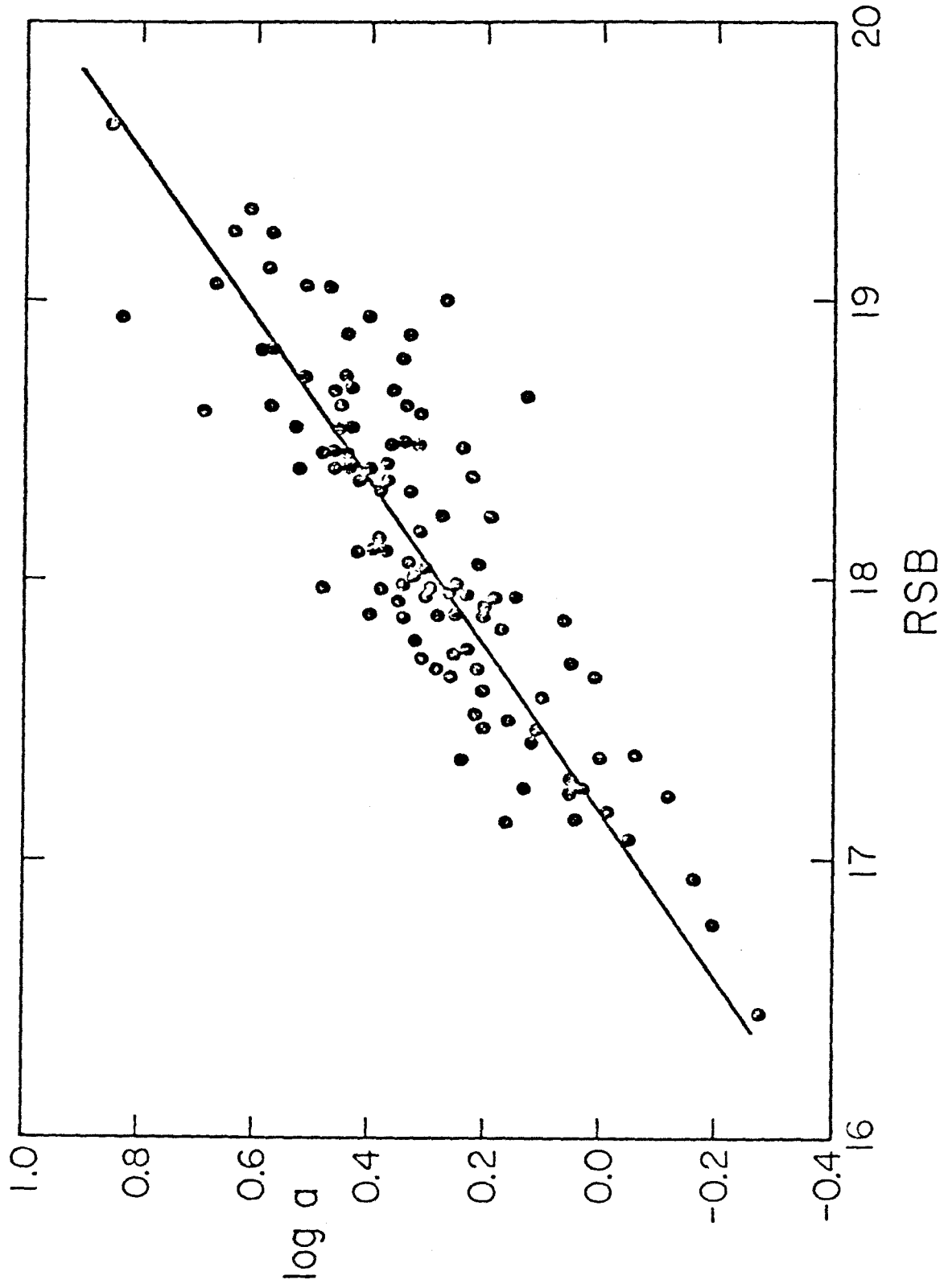
1.0
0.8
0.6
0.4
0.2
0.0
-0.2
-0.4
log a
16
17
18
19
20
RSB